
Prediction-Centric Uncertainty Quantification via MMD

Zheyang Shen
Newcastle University

Jeremias Knoblauch
University College London

Sam Power
University of Bristol

Chris. J. Oates
Newcastle University

Abstract

Deterministic mathematical models, such as those specified via differential equations, are a powerful tool to communicate scientific insight. However, such models are necessarily simplified descriptions of the real world. Generalised Bayesian methodologies have been proposed for inference with misspecified models, but these are typically associated with vanishing parameter uncertainty as more data are observed. In the context of a misspecified deterministic mathematical model, this has the undesirable consequence that posterior predictions become deterministic and certain, while being incorrect. Taking this observation as a starting point, we propose *Prediction-Centric Uncertainty Quantification*, where a mixture distribution based on the deterministic model confers improved uncertainty quantification in the predictive context. Computation of the mixing distribution is cast as a (regularised) gradient flow of the maximum mean discrepancy (MMD), enabling consistent numerical approximations to be obtained. Results are reported on both a toy model from population ecology and a real model of protein signalling in cell biology.

world. This can lead to misleading inferences and predictions, and is a particular problem across disciplines as diverse as climatology, epidemiology, and cell biology, where deterministic and simulation-based models are routinely used [see Hermans et al., 2022].

A naïve and often reflexive remedy proposed for addressing such robustness concerns is (some form of) Bayesian inference [e.g., Beaumont, 2010, Csilléry et al., 2010]. Here, the hope is that the influence of a well-specified prior, coupled with an appropriate measurement error model, can counteract the failure to model the often complex structure that remains in the residual. Unfortunately, this approach is flawed: As more data are observed, the influence of the prior is diminished and the Bayesian posterior concentrates around a single best-fitting parameter value [see e.g., Ghosal et al., 2000, Van der Vaart, 2000, Ghosal and van der Vaart, 2007]. This loss of epistemic uncertainty is a severe limitation, as being pushed towards placing all belief on a singular parameter value leads to arbitrarily confident deterministic predictions being generated under a model that is fundamentally misspecified.

Despite considerable research into robust and/or generalised Bayesian inference, it remains the case that virtually all existing methodologies suffer the same problem: While they provide robustness in the face of misspecified observations, noise, and outliers, their posteriors still collapse towards a single best-fitting parameter value once sufficient data are observed [see Chernozhukov and Hong, 2003, Miller, 2021, Matsubara et al., 2022, 2024, Frazier et al., 2024]. To bridge the gap between powerful deterministic modelling and probabilistic uncertainty quantification, a change in perspective may be required.

This paper presents a new approach to probabilistic inference and prediction in the context of misspecified deterministic mathematical models, capable of providing non-vanishing epistemic uncertainty as more data are observed. This is achieved by inducing uncertainty in the parameter space through the implied predictive model, which is now interpreted as a mixture component within a mixture model. A variational crite-

1 INTRODUCTION

Deterministic modelling has long been a staple in scientific and engineering disciplines, providing a simplified yet powerful framework in which complex systems can be understood. Unfortunately, such models are typically misspecified and, by their very nature, do not attempt to capture more complex aspects of the real

tion is proposed, based on the *maximum mean discrepancy* (MMD), which provides robustness to data outliers and enables computation via (regularised) gradient flow of the MMD. Practically, the result is an interacting particle system whose limiting distribution quantifies parameter uncertainty in a manner that is relevant to the predictive context. As we show in a range of experiments, this new methodology is particularly appealing when one fits noisy data to a deterministic and possibly misspecified mathematical model.

2 MOTIVATION

Bayesian inference is often promoted as a silver bullet for epistemic uncertainty quantification. However, to produce well-calibrated uncertainty, Bayesian updating requires the likelihood function to be well-specified [Walker, 2013, Bissiri et al., 2016]. This is rarely the case when working with a deterministic mathematical model, as properly acknowledging the complexities of real-world data almost always requires stochasticity to feature at some level in the model. The situation is not easily resolved, as from a scientific modelling point of view it can be much more challenging to design an accurate stochastic model compared to using traditional established techniques to design an interpretable deterministic model.

A naïve remedy would be to replace parameter inference and prediction with a form of—possibly black box—density estimation [e.g. Fong et al., 2023]. Unfortunately, this would not be a useful solution in many scientific enquiries, as the structure provided by even an approximate model can be essential in constraining predictions to be at least ‘in the right ballpark’. Further, many mathematical models are explicitly *causal* models; for example, a differential equation model of cell signalling may describe biological mechanisms governing the signalling dynamics. A causal model enables prediction for the effect of interventions which change how the system operates, such as the use of molecular drug treatment to modulate cell signalling (an example is presented in Section 6.2), which density estimation alone cannot.

A second angle of attack that may seem appealing at first glance is to appeal to generalised Bayesian methods [Knoblauch et al., 2022]. These can produce posteriors that are robust to outliers when the data-generating model is misspecified—a feature that is particularly pertinent to deterministic mathematical models. Yet, these methods exhibit a limitation similar to Bayesian inference, in that parameter uncertainty vanishes as more data are observed. This is due to the fact that generalised Bayesian procedures quantify parameter uncertainty in relation to the fit

of data to a general loss function—rather than the implied predictive distribution on observables. Such behaviour might be desirable if the data-generating mechanism perfectly aligns with a specific parameter value of the posited model, but it significantly worsens the predictive capacity of deterministic models that are misspecified, as incorrect predictions can become arbitrarily confident when more and more data are collected. This could in principle have serious real-world implications; for example, in Section 6.2 we present a case study in which over-confidence in the efficacy of a drug treatment results from applying Bayesian and generalised Bayesian methods to a misspecified deterministic cell signalling model.

3 PREDICTION-CENTRIC UNCERTAINTY

This section describes our *prediction-centric* perspective on inference and prediction with a (possibly misspecified) deterministic mathematical model. As with Bayesian and generalised Bayesian procedures, the approach that we present next produces a distribution over parameter values as its output. However, unlike these existing approaches, the parameter uncertainty in our methodology will not be defined relative to the *average data fit* of the model, but relative to its *predictive fit* instead.

Our inspiration is drawn from the optimisation-centric view on Bayesian inference, in line with many contemporary extensions of Bayesian reasoning [Knoblauch et al., 2022]. To explain this perspective, we define the parameter space Θ , and consider observations $y_i \in \mathcal{Y}$ for $i = 1, 2, \dots, n$ with $y_{1:n} = (y_1, y_2, \dots, y_n)$, eschewing all considerations of measurability to simplify presentation throughout. The unsuitability of a given parameter $\theta \in \Theta$ for the observations $y_{1:n} \in \mathcal{Y}^n$ is quantified by a *loss function* $\mathcal{L}_n : \Theta \times \mathcal{Y}^n \rightarrow \mathbb{R}$. Further, we denote by $\mathcal{P}(\Theta)$ the set of probability distributions on Θ , by $Q_0 \in \mathcal{P}(\Theta)$ a prior probability distribution over Θ , by $\text{KL}(Q, P)$ the *Kullback–Leibler* (KL) divergence between two probability distributions $Q, P \in \mathcal{P}(\Theta)$, and by $\lambda_n > 0$ a scalar. In Knoblauch et al. [2022], it is argued that a principled recipe for obtaining (generalised) posteriors over Θ is given by the (assuming uniqueness) minimiser

$$Q_n^\dagger = \arg \min_{Q \in \mathcal{P}(\Theta)} \underbrace{\int \mathcal{L}_n(\theta, y_{1:n}) dQ(\theta)}_{\text{average data fit}} + \underbrace{\lambda_n \text{KL}(Q, Q_0)}_{\text{regularisation}}, \quad (1)$$

which recovers the standard Bayesian posterior distribution when $\mathcal{L}_n(\theta, y_{1:n}) = -\log p_\theta(y_{1:n})$ is the negative log-likelihood arising from a statistical model $P_\theta \in \mathcal{P}(\mathcal{Y})$, and $\lambda_n = 1$. In the motivating con-

text of deterministic mathematical models, the *statistical* model P_θ might represent noise-corrupted observations of the deterministic model output. For various other choices of \mathbf{L}_n and λ_n , generalised Bayesian methods can produce robust posteriors suitable for dealing with certain forms of statistical model misspecification [see Hooker and Vidyashankar, 2014, Ghosh and Basu, 2016, Knoblauch et al., 2018, Schmon et al., 2020, Chérif-Abdellatif and Alquier, 2020, Dellaporta et al., 2022, Husain and Knoblauch, 2022, Altamirano et al., 2023, 2024, Duran-Martin et al., 2024].

For all reasonable choices of \mathbf{L}_n and λ_n , the relative importance of the first term in (1) increases with n . As a result, Q_n^\dagger increasingly allocates most of its probability mass around a single (assuming uniqueness) best-fitting parameter θ^\dagger [Miller, 2021]. This effect is particularly problematic if the loss is defined relative to a parameter θ that indexes a misspecified model P_θ : now, the implied posterior predictive $\int P_\theta dQ_n^\dagger(\theta)$ will quickly collapse to the plug-in predictive P_{θ^\dagger} , and will effectively predict from a singular element of the misspecified model class $\{P_\theta : \theta \in \Theta\}$. As a result, posteriors Q_n^\dagger computed via (1) will exhibit poor predictive uncertainty. For a formal proof and additional findings surrounding this phenomenon, we refer the reader to McLatchie et al. [2024].

To remedy the predictive drawbacks of generalised Bayesian methods, we develop an alternative approach that instead quantifies parameter uncertainty relative to *predictive* capability, and replaces the role of the average data fit with a form of predictive fit. To achieve this, we first denote the *maximum mean discrepancy* (MMD) between probability distributions P, Q as $\text{MMD}(P, Q)$ [see e.g. Gretton et al., 2012], and denote the empirical measure of the dataset as $P_n = \frac{1}{n} \sum_{i=1}^n \delta_{y_i}$. Then we compute the (assuming uniqueness) minimiser

$$Q_n = \arg \min_{Q \in \mathcal{P}(\Theta)} \underbrace{\frac{1}{2} \text{MMD}^2(P_n, Q)}_{\text{predictive fit}} + \underbrace{\lambda_n \text{KL}(Q, Q_0)}_{\text{regularisation}} \quad (2)$$

where

$$P_Q = \int P_\theta dQ(\theta) \in \mathcal{P}(\mathcal{Y}) \quad (3)$$

denotes a mixture model, whose components are instances P_θ of the statistical model and whose mixing distribution is Q , and $\lambda_n > 0$ a constant to be specified. Throughout the remainder of this paper, procedures defined by minimising (2) will be referred to as *Prediction-Centric Uncertainty Quantification* (PCUQ). Before discussing related work, we briefly comment on the main features of PCUQ:

Mixture Model The mixture model P_Q in (3) expands predictive potential beyond the original statis-

tical model P_θ , which may be useful if the original statistical model is misspecified. On the other hand, P_Q retains the original statistical model P_θ as the special case where $Q = \delta_\theta$, which in principle enables P_θ to be exploited when the model is well-specified.

Predictive Fit The use of MMD in (2), as opposed to other statistical divergences, confers outlier-robustness to PCUQ, which may be valuable in the misspecified context (c.f. Section 5.2), and the use of the *squared* MMD carries computational advantages, enabling the use of powerful emerging sampling methods based on gradient flows [Wild et al., 2023] (c.f. Section 5.3).

Regularisation Similarly to (1), the regularisation term involves a reference distribution Q_0 (i.e. the prior, in the standard Bayesian context). The functional role of Q_0 in PCUQ is explored in Appendix A, where we derive the perhaps surprising result that Q_0 acts on Q_n in essentially the same way that Q_0 acts on Gibbs measures like Q_n^\dagger , as a reference measure in a Radon–Nikodym derivative [Bissiri et al., 2016, Knoblauch et al., 2022] (c.f. Theorem 2 in Appendix A). That is, one can reason about ‘updating belief distributions’ using PCUQ.

4 RELATED WORK

The ideas we pursue in this work are linked to, and in some ways improve upon, a collection of seemingly disparate previous contributions in both classical statistics and machine learning.

First amongst these is *nonparametric maximum likelihood*, which minimises $Q \mapsto -\frac{1}{n} \sum_{i=1}^n \log p_Q(y_i)$ where p_Q is a density for P_Q [see Chapter 5 of Lindsay, 1995]. This objective approximates $\text{KL}(P_\star, P_Q)$ when $y_{1:n}$ is a collection of n independent samples from $P_\star \in \mathcal{P}(\mathcal{Y})$, and can therefore be interpreted as a version of (2) where $\lambda_n = 0$ and MMD^2 is replaced by KL . The lack of regularisation causes several issues, including computational difficulties and non-identifiability [see e.g. Laird, 1978], as the minimising measure will generally be fully atomic, see Lindsay [1995, e.g. Theorem 21 in Chapter 5] and Jordan-Squire [2015].

One way of addressing these shortcomings is via regularisation. While the link to nonparametric maximum likelihood is never explicit, regularisation like this has been enforced by adding a KL divergence as in (2) and by constraining Q to a parametric variational family \mathcal{Q} [Jankowiak et al., 2020b,a, Sheth and Kharon, 2020],

resulting in objectives that are variants of

$$\arg \min_{Q \in \mathcal{Q}} -\frac{1}{n} \sum_{i=1}^n \log(p_Q(y_i)^\alpha) + \lambda_n \text{KL}(Q, Q_0). \quad (4)$$

For example, the choice $\lambda_n = \frac{\alpha}{n}$ can be linked to approximation of the standard Bayesian posterior via α -divergences Li and Gal [2017], Villacampa-Calvo and Hernandez-Lobato [2020]. Similarly, this objective has been considered in the context of Gaussian processes and deep Gaussian processes with $\alpha = 1$ and various choices for λ_n Jankowiak et al. [2020a,b], Sheth and Khardon [2020]. More recently, Crucinio et al. [2024] used a similar formulation to solve Fredholm integral equations. Enriching this with a solid theoretical foundation, Masegosa [2020] and Morningstar et al. [2022] motivated targeting objectives like (4) via PAC-Bayesian bounds. While they result in superior predictive performance relative to standard Bayesian and variational schemes, the applicability of objectives like (4) is limited; apart from Gaussian-type likelihoods where the log integral $\log p_Q(y_i)$ has a closed form, computation can become impractical. In particular, approximating the log integral via samples from Q can yield a highly biased approximation, and generally renders this methodology impractical.

This substantive drawback prompts us to seek inspiration from an ongoing line of research into generalised and post-Bayesian methods (1) popularised by Bisiri et al. [2016] and Knoblauch et al. [2022]. Specifically, we will go beyond loss functions that focus on goodness-of-fit, and instead assess predictive fit. Further, we seek a predictive loss that is both computationally feasible and robust. To achieve this, we follow Chérif-Abdellatif and Alquier [2020] and Alquier and Gerber [2024], and assess predictive fit in (2) via the (squared) MMD. Beyond tackling the computational challenges of the intractable log integral $\log p_Q(y_i)$, the MMD allows us to obtain inferences that are more robust to outliers and model misspecification [see Briol et al., 2019a, Chérif-Abdellatif and Alquier, 2022, Alquier et al., 2023].

5 METHODOLOGY

Throughout Sections 5.1 to 5.3, we will simplify the presentation and assume that y_i are sampled independently from some unknown population distribution $P_\star \in \mathcal{P}(\mathcal{Y})$. The case of non-independent data, where data y_i are allowed to depend on covariates x_i , is deferred to Section 5.4.

5.1 Predictive Fit via MMD

The predictive fit term in (2) is based on the MMD, which will simultaneously confer computational effi-

ciency and robustness to our method. To define it, we let $k : \mathcal{Y} \times \mathcal{Y} \rightarrow \mathbb{R}$ be a kernel¹ and denote by $\mathcal{H}(k)$ the associated *reproducing kernel Hilbert space* (RKHS) [see Berlinet and Thomas-Agnan, 2011, for background]. For a given kernel k and a probability distribution $P \in \mathcal{P}(\mathcal{Y})$, we can now define the *kernel mean embedding* as²

$$\mu_k(P) := \int k(\cdot, y) dP(y) \in \mathcal{H}(k).$$

The divergence of a candidate $P \in \mathcal{P}(\mathcal{Y})$ from the data-generating distribution P_\star can be quantified using MMD; a pseudometric defined as the RKHS-norm between the pair of kernel mean embeddings, i.e.

$$\text{MMD}(P_\star, P) = \|\mu_k(P_\star) - \mu_k(P)\|_{\mathcal{H}(k)}.$$

The MMD is a proper metric if k is a *characteristic* kernel [Sriperumbudur et al., 2011]; our use of MMD is justified by its interpretation as a statistical divergence induced by a *proper scoring rule* [Dawid, 1986]. The mixture model P_Q in (2) has kernel mean embedding

$$\mu_k(P_Q) = \iint k(\cdot, y) dP_\theta(y) dQ(\theta) = \int \mu_k(P_\theta) dQ(\theta),$$

so the MMD between P_\star and P_Q can be written as

$$\begin{aligned} \text{MMD}^2(P_\star, P_Q) &= \left\| \int \{\mu_k(P_\star) - \mu_k(P_\theta)\} dQ(\theta) \right\|_{\mathcal{H}(k)}^2 \\ &= \iint \kappa_{P_\star}(\theta, \vartheta) dQ(\theta) dQ(\vartheta), \end{aligned} \quad (5)$$

where the last step follows from expanding the norm, using the inner product, and exchanging inner product and integral. Here, the resulting $\kappa_{P_\star} : \Theta \times \Theta \rightarrow \mathbb{R}$ is a kernel on Θ , and given by

$$\kappa_{P_\star}(\theta, \vartheta) = \langle \mu_k(P_\star) - \mu_k(P_\theta), \mu_k(P_\star) - \mu_k(P_\vartheta) \rangle_{\mathcal{H}(k)}.$$

This reveals one possible interpretation of (5) as a *kernel Stein discrepancy* [Chwialkowski et al., 2016, Liu et al., 2016, Gorham and Mackey, 2017] corresponding to the *Stein kernel* κ_{P_\star} [Oates et al., 2017]. One of the implications is that, if $P_\star = P_{\theta_\star}$ for some unique $\theta_\star \in \Theta$, then (5) is uniquely minimised by $Q = \delta_{\theta_\star}$ provided k is a characteristic kernel.

5.2 Estimation, Regularisation and Robustness

Of course, the true data-generating distribution P_\star in (5) is unknown and must be approximated. Following

¹A function $k : \mathcal{Y} \times \mathcal{Y} \rightarrow \mathbb{R}$ is a *kernel* if $k(u, v) = k(v, u)$ for all $u, v \in \mathcal{Y}$, and $\sum_{i=1}^m \sum_{j=1}^m w_i w_j k(u_i, u_j) \geq 0$ for all $w_1, \dots, w_m \in \mathbb{R}$, $u_1, \dots, u_m \in \mathcal{Y}$, and $m \in \mathbb{N}$.

²Throughout, we will assume this embedding exists as a strong (Bochner) integral. This always holds for the most popular choices of kernels (such as Gaussian and Matérn kernels).

(2), we use the empirical distribution P_n in lieu of P_\star . For this special case, we find

$$\kappa_{P_n}(\theta, \vartheta) \stackrel{+C}{=} \iint k(y, y') dP_\theta(y) dP_\vartheta(y') - \frac{1}{n} \sum_{i=1}^n \int k(y_i, y) dP_\theta(y) - \frac{1}{n} \sum_{i=1}^n \int k(y_i, y) dP_\vartheta(y), \quad (6)$$

where $\stackrel{+C}{=}$ denotes a θ - and ϑ -independent additive constant. Specific choices of k and P_θ lead to tractable integrals in (6), while computational strategies are available when numerical approximation is required; see Appendix B.1. One can contrast the bias introduced in the Monte Carlo approximation of log integrals $\log p_Q(y_i)$ that occurs in approximating objectives of the family in (4) with straight-forward unbiased approximation of the squared MMD via Monte Carlo. Further, Huber robustness of the MMD is immediate from (6), since outlier data y_i far from the effective support of P_θ contribute negligibly to (6) for typical choice of kernel k [Alquier and Gerber, 2024].

A plug-in approximation necessitates additional regularisation, since otherwise minimisation of $Q \mapsto \text{MMD}(P_n, P_Q)$ would result in a discrete distribution where, similarly to nonparametric maximum likelihood, each atom in the support would correspond to a value of θ that explains one of the data points well. One naïve possibility for the regulariser is to use another (squared) MMD between Q and a reference distribution $Q_0 \in \mathcal{P}(\Theta)$. This choice is appealing because it is again a quadratic form, so efficient convexity-exploiting algorithms can be used. However, the (squared) MMD regulariser imposes a weak topology that is prone to the same issue of returning a distribution with finite support, and does not impose sufficient convexity for the gradient flow algorithms described in Section 5.3 to converge [this was proven in Theorem 6 of Wild et al., 2023]. Instead, we choose to employ KL regularisation in (2), which ensures that Q_n is absolutely continuous with respect to Q_0 (c.f. Theorem 2 in Appendix A).

The main challenge with using KL regularisation in this context is that, until very recently, there were not efficient computational algorithms for solving regularised variational problems such as (2). Fortunately, recent work on gradient flows provides a path forward Wild et al. [2023], which we explain next.

5.3 Approximating Q_n via Gradient Flow

From (2), and now with $\Theta = \mathbb{R}^p$, the output Q_n of the proposed PCUQ method is a minimiser of the entropy-regularised objective

$$\mathcal{F}_n(Q) = \mathcal{E}_n(Q) + \lambda_n \int \log q(\theta) dQ(\theta), \quad (7)$$

where the *free energy* $\mathcal{E}_n(Q)$ is identical, after algebraic manipulation, to

$$\mathcal{E}_n(Q) \stackrel{+C}{=} \int v(\theta) dQ(\theta) + \frac{1}{2} \iint \kappa_{P_n}(\theta, \vartheta) dQ(\theta) dQ(\vartheta),$$

where $v(\theta) = -\lambda_n \log q_0(\theta)$, and where q and q_0 are respectively densities for Q and Q_0 . Sufficient conditions for existence and uniqueness of Q_n , for any choice of $\lambda_n > 0$, are presented in Theorem 1 of Appendix A. Based on this perspective, we can exploit recent advances in mean-field Langevin dynamics to numerically approximate Q_n , as we explain next.

For the entropy-regularised functional \mathcal{F}_n (7), we can simulate a Wasserstein gradient flow via a McKean–Vlasov process [Ambrosio et al., 2008]

$$d\theta_t = -\nabla_W \mathcal{E}_n(Q^t)(\theta_t) + \sqrt{2\lambda_n} dW_t, \quad (8)$$

$$\nabla_W \mathcal{E}_n(Q^t)(\theta_t) = \nabla v(\theta_t) + \int \nabla_1 \kappa_{P_n}(\theta_t, \vartheta) dQ^t(\vartheta)$$

where $Q^t = \text{law}(\theta_t)$, ∇_W denotes the Wasserstein gradient, $(W_t)_{t \geq 0}$ is a Wiener process on \mathbb{R}^p and, for the bivariate function κ_{P_n} , the notation $\nabla_1 \kappa_{P_n}$ denotes differentiation with respect to the first argument. As (8) can be seen as the mean-field limit of an interacting particle system, we can discretise Q^t into a system of N evolving particles $\theta_t^1, \theta_t^2, \dots, \theta_t^N$, whose evolution is governed by the following system of *stochastic differential equations* (SDEs):

$$d\theta_t^i = - \left(\nabla v(\theta_t^i) + \frac{1}{N-1} \sum_{j \neq i} \nabla_1 \kappa_{P_n}(\theta_t^i, \theta_t^j) \right) dt + \sqrt{2\lambda_n} dW_t^i, \quad (9)$$

where $(W_t^i)_{t \geq 0}$ are N independent Wiener processes on \mathbb{R}^p . An Euler–Maruyama discretisation of (9) incurs per-iteration computational complexity $O(nN^2)$ and storage complexity (with caching) of $O(n + N)$. The only remaining technical challenge in simulating (9) is calculation of the gradient $\nabla_1 \kappa_{P_n}$; this mirrors the challenge of evaluating the integrals defining κ_{P_n} itself in (6), and the same strategies discussed in Appendix B.1 can be applied.

Gradient flows are preferred in this paper for their ease of implementation, but other computational methods could be considered; see Appendix C.

5.4 Extension to Dependent Data

Consider now the (often more practically-relevant) setting of non-independent data, where each datum y_i is associated with a covariate $x_i \in \mathcal{X}$ and generated according to an (unknown) conditional distribution $P_\star(\cdot | x_i)$. Our task now involves a conditional model

$\{P_\theta(\cdot|x)\}_{\theta \in \Theta}$ for each $x \in \mathcal{X}$. To extend our methodology to this setting, we suppose that

$$\{(x_i, y_i)\}_{i=1}^n \stackrel{\text{iid}}{\sim} \bar{P}_*(dx, dy) := \frac{1}{n} \sum_{i=1}^n \delta_{x_i}(dx) P_0(dy|x_i)$$

and consider the extended model

$$\bar{P}_\theta(dx, dy) := \frac{1}{n} \sum_{i=1}^n \delta_{x_i}(dx) P_\theta(dy|x_i) \quad (10)$$

so that $\bar{P}_*, \bar{P}_\theta \in \mathcal{P}(\mathcal{X} \times \mathcal{Y})$. Our approach then proceeds as before, but with k now a kernel on the extended space $\mathcal{X} \times \mathcal{Y}$. For example, if $\mathcal{X} \subset \mathbb{R}^{d_x}$ and $\mathcal{Y} \subset \mathbb{R}^{d_y}$, we may consider the Gaussian kernel

$$k((x, y), (x', y')) = \exp\left(-\frac{\|x - x'\|^2}{\ell_{\mathcal{X}}^2} - \frac{\|y - y'\|^2}{\ell_{\mathcal{Y}}^2}\right) \quad (11)$$

with bandwidths $\ell_{\mathcal{X}}$ and $\ell_{\mathcal{Y}}$ to be specified. The lifting of a conditional density to a joint density via a *plug-in* empirical distribution for the covariate was studied in Alquier and Gerber [2024]. The suitability of this approach hinges on the number n of data being sufficiently large, and the characteristics of the dependence on covariates being appropriately modelled by the kernel. The latter assumption can be removed by formally taking $\ell_{\mathcal{X}} \rightarrow 0$, as recommended in Alquier and Gerber [2024]. Strategies for numerically approximating $\nabla_1 \kappa_{P_n}$ extend to this non-independent setting; details are deferred to Appendix B.2. A reduction in computational complexity also results from taking the $\ell_{\mathcal{X}} \rightarrow 0$ limit; see Appendix B.3.

6 EXPERIMENTS

For empirical assessment, we focus on the notable failure of standard and generalised Bayesian inference in the context of misspecified deterministic *ordinary differential equation* (ODE) models, asking whether the situation can be improved using PCUQ. Examples of this abound; here we consider (a) the canonical Lotka–Volterra ODE model from population ecology, as a simple test-bed where the failure of Bayesian inference can be easily understood (Section 6.1), and (b) a sophisticated system of ODEs describing a cell signalling pathway, where prediction of cell response to a molecular treatment is required (Section 6.2). All experiments were performed on a 2023 MacBook Pro with 16 GB RAM. Code to reproduce these experiments can be downloaded from https://github.com/zheyang-shen/prediction_centric_uq.

6.1 Illustration on a Lotka–Volterra Model

As a simple test bed, we consider inference and prediction based on the deterministic *Lotka–Volterra model*

(LVM) in a context where data actually arise from a stochastically modified LVM.

Lotka–Volterra Model As a prototypical model from population ecology, the LVM describes the dynamical interaction between a prey (u_1) and predator (u_2) as a coupled system of differential equations

$$\begin{aligned} \frac{du_1}{dx} &= \alpha u_1 - \beta u_1 u_2, & u_1(0) &= \xi_1, \\ \frac{du_2}{dx} &= \delta u_1 u_2 - \gamma u_2, & u_2(0) &= \xi_2, \end{aligned}$$

for some $\alpha, \beta, \gamma, \delta, \xi_1, \xi_2 \geq 0$. Real data arise as noisy observations of one or more species at discrete times; for our purposes we suppose that $y_{1:n}$ are noisy measurements of the populations $u = (u_1, u_2)$ at times $x_{1:n}$. It is common to fit such models to data via the assumption of a Gaussian likelihood, which in this case would correspond to a Gaussian model with density

$$p_\theta(y_i|x_i) = \prod_{i=1}^n \frac{1}{\sqrt{2\pi\sigma^2}} \exp\left(-\frac{\|y_i - u_\theta(x_i)\|^2}{2\sigma^2}\right), \quad (12)$$

where parameters are $(\alpha, \beta, \gamma, \delta, \xi_1, \xi_2, \sigma)$, and we denote the dependence of the prey and predator populations on these parameters using u_θ . To improve visualisation, we consider inference only for $\theta_1 := \text{logit}(\alpha)$ and $\theta_2 = \text{logit}(\beta)$, with all other parameters fixed. The distribution Q_0 was taken to be standard normal.

Failure of Bayesian Inference To explore the pitfalls of Bayesian inference when the LVM is misspecified, we simulated predator-prey interactions using both the above ODE and a stochastic LVM ($\epsilon_1, \epsilon_2 > 0$):

$$\begin{aligned} du_1 &= (\alpha u_1 - \beta u_1 u_2) dx + \epsilon_1 dW_1, & u_1(0) &= \xi_1, \\ du_2 &= (\delta u_1 u_2 - \gamma u_2) dx + \epsilon_2 dW_2, & u_2(0) &= \xi_2, \end{aligned}$$

where stochasticity is used to represent the additional complexities of real predator-prey interactions that are not explicitly captured by the simple ODE model. Observation noise was added to these simulations using the same Gaussian model in (12), so that the observation model (at least) is correctly specified. The values of all parameters are given in Appendix E.1.

Bayesian inference is seen to work well when the model is well-specified, but to fail when predicting future predator and prey abundance when the model is misspecified. This is because the Bayesian posterior concentrates around a single parameter configuration (Figure 1, top left panel), leading to concentration of the predictive distribution for $u(x)$ (Figure 1, middle column). Yet future predator and prey abundances do not coincide with these predicted values when the

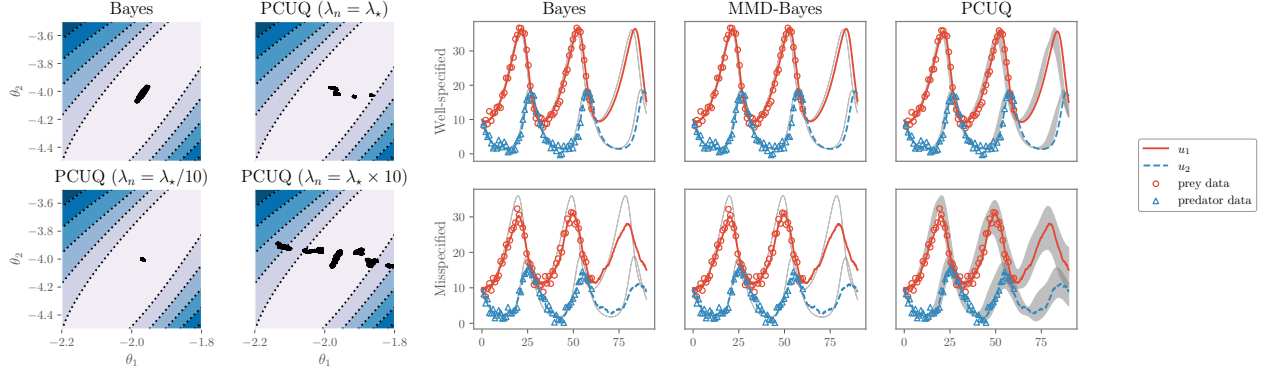


Figure 1: Lotka–Volterra model. Left: Contour plots depict the standard Bayesian posterior, superimposed with samples from the standard Bayesian posterior (Bayes) and the proposed method (PCUQ) with varying regularisation parameter λ_n . Right: Predictive distributions in both the well-specified (top) and misspecified (bottom) context. (Lines depict true prey and predator populations, while the shaded regions depict the predictive quartiles for standard Bayesian inference, the MMD-Bayes method of Chérif-Abdellatif and Alquier [2020], and the proposed PCUQ.)

model is misspecified, rendering the Bayesian posterior grossly over-confident. The same failure mode occurs for generalised Bayesian methods, which also concentrate around a single parameter. We illustrate this using the example of MMD-Bayes [Chérif-Abdellatif and Alquier, 2020], in the fourth column of Figure 1 (for details, see Appendix E.1).

Prediction-Centric UQ Performing PCUQ in this context requires the extension to dependent data described in Section 5.4. The Gaussian kernel (11) was employed with bandwidths $\ell_X \rightarrow 0$ and $\ell_Y = \sigma$ following the recommendation in Alquier and Gerber [2024]; further discussion is contained in Appendix B.3. The Gaussian kernel has the distinct advantage that all of the integrals appearing in (6) can be analytically evaluated, due to conjugacy with the Gaussian measurement error model (12); see Appendix D. The regulariser λ_n was set to the value λ_* for which the spread of the PCUQ output Q_n was similar to that of the standard Bayesian posterior Q_n^\dagger when the model is well-specified (see Figure 1, left); a generally-applicable heuristic³ that requires only simulating data from the statistical model. Since this system of ODEs does not admit a closed-form solution, we solve the sensitivity equations to compute the gradients $\nabla_\theta \log p_\theta(y_i|x_i)$ as required to implement the gradient flow (9). The predictive output from PCUQ, obtained with a particle system of size $N = 10$, is displayed in the right column of Figure 1. This is qualitatively distinct

from the standard Bayesian posterior, as would be expected. Using PCUQ, the over-confidence of existing methodologies in the misspecified context is seen to be avoided. Convergence diagnostics for the gradient flow are presented in Figure 3 and insensitivity of the predictions to increasing N and decreasing λ_* is demonstrated in Figures 4 to 6, all contained in Appendix E.1.

6.2 Model Misspecification in Cell Signalling

Systems biology is ripe for PCUQ, since the community has invested decades of effort into the design of detailed ODE descriptions of cellular signalling pathways, with thousands of models hosted on repositories such as BioModels [Malik-Sheriff et al., 2020]. The sheer complexity of cellular signalling necessarily means that such models are misspecified, yet they continue to serve as valuable tools to communicate understanding and can usefully constrain causal predictions to some extent [Alon, 2019]. Our contention is that appropriate methodology to harness the predictive performance of such misspecified ODEs within a probabilistic framework does not yet exist, but can be provided by PCUQ. To support this argument, we present a case study in which a detailed ODE description of *extracellular signal regulated kinase* (ERK) signalling is used to predict cellular response to a molecular treatment.

Adopting a similar notation and set-up as Section 6.1, the evolution of concentrations of molecular species was modelled as the solution $x \mapsto u_\theta(x) \in \mathbb{R}^{d_Y}$ to a system of $d_Y = 11$ ODEs, with parameters collectively denoted $\theta \in \mathbb{R}^p$, $p = 11$. Data were gener-

³A heuristic is necessary, as strategies for selecting λ_n in generalised Bayesian methods remain a subject of ongoing research and debate, as discussed in detail in Wu and Martin [2023], McLatchie et al. [2024]. Advances in this direction could potentially be deployed to PCUQ.

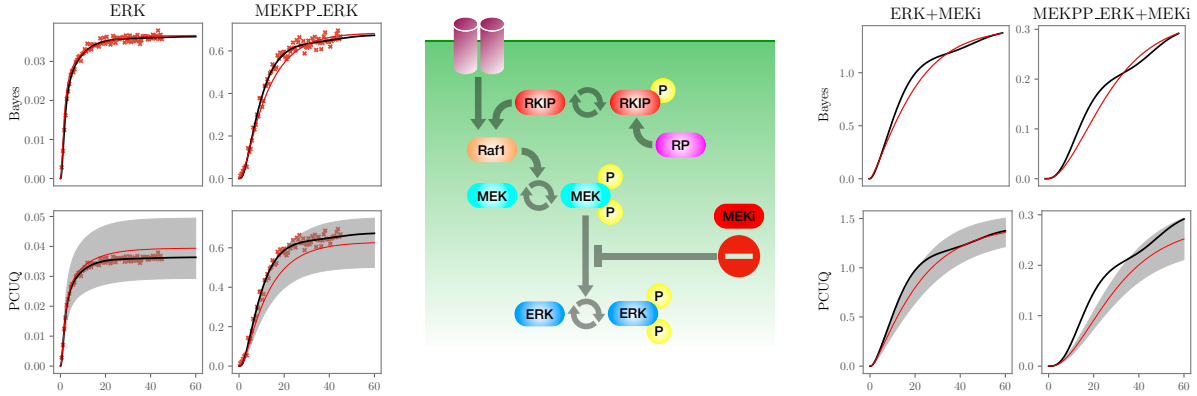


Figure 2: ERK signalling model (centre); this system of 11 ODEs is necessarily misspecified. Data (red crosses) were obtained as noisy observations of the system trajectory (black line) in an observational regime (left), and the task was to predict the causal effect of a MEK inhibitor (MEKi) on ERK signalling. Predictions (right) produced using standard Bayesian inference (top row) were over-confident, while PCUQ (bottom row) enabled predictive uncertainty to be accurately quantified. (Here the red line indicates predictive mean, while the shaded region indicates predictive quartiles.)

ated by adding independent Gaussian noise (variance $\sigma^2 I_{11 \times 11}$) to the true molecular concentrations $u(x)$ at discrete times $x_{1:n}$. The true molecular concentrations $u(x)$ were simulated from the same model, but where the propensity for molecular interaction was no longer constant but time-varying, reflecting the complexity of the cellular environment; full details are contained in Appendix E.2. For PCUQ, the kernel k , bandwidths, and regularisation parameter λ_n were all selected using the same approach used in Section 6.1.

As the scientific task, we seek to predict the evolution of ERK under the application of the *MEK inhibitor* (MEKi), depicted in the centre panel of Figure 2. Such interventional data were not part of the training dataset, but as an explicitly causal mechanistic model it is possible to make a causal prediction regarding cell response to treatment⁴. Predictions made using standard Bayesian inference are contrasted to the predictions made using PCUQ in Figure 2. Failure of Bayesian inference has occurred in an analogous manner to that described in Section 6.1, with the potentially serious consequence that uncertainty in the efficacy of the MEKi treatment is under-reported (indeed, predictive uncertainty is barely visible in the plot). In contrast, predictive over-confidence has been avoided through the use of PCUQ.

⁴Briefly, MEKi prevents binding of phosphorylated MEK to ERK (the complex being denoted MEKPP.ERK), increasing the concentration of free ERK relative to pre-treatment.

7 Discussion

Deterministic models are an important scientific tool for communicating understanding and insight, but their use in a statistical context typically results in a model that is misspecified. In a limited data context, the presence of misspecification can often be neglected. However, model misspecification typically becomes the leading contributor to prediction error as more data are obtained. Existing (generalised) Bayesian methods are unable to calibrate their predictive confidence in this large data limit, with arbitrarily high confidence associated to a prediction that is incorrect.

This paper proposes a possible solution, called PCUQ. The central idea is to replace the usual notion of *average data fit* with a new notion of *predictive fit*. Operationalising this idea via MMD and gradient flows, we demonstrated that catastrophic over-confidence can be avoided in two exemplar ODE models. Our work suggests several new directions for future work: (i) analysing convergence of the particle-discretised gradient flow, following e.g. Chizat [2022], Hu et al. [2021], Nitanda et al. [2022]; (ii) obtaining theoretical insight into the selection of λ_n ; and (iii) obtaining guarantees on the coverage of Q_n when the model is well-specified, in particular accounting for the plug-in approximation (10) in the case where data are dependent.

The issue of a misspecified deterministic model is not itself new, and methods that attempt to *learn the residual* date back at least to Kennedy and O’Hagan [2001]. These methods are also prediction-centric, but they sacrifice any causal semantics associated to the statistical model by modifying the model itself,

through the introduction of a nonparametric component. A key distinguishing feature of PCUQ is that, while being prediction-centric, causal semantics associated to the model are retained. On the negative side, this means that (possibly causal) predictions made using PCUQ are ultimately gated by the performance of the original statistical model. This highlights the scale of the challenge associated with model misspecification; an area where substantial further work is required.

Acknowledgements

The authors are grateful to Joshua Bon, Aidan Mullins, and Veit Wild for discussion of earlier work. ZS and CJO were supported by EP/W019590/1. CJO acknowledges support from The Alan Turing Institute in the UK. JK was supported through the UK's Engineering and Physical Sciences Research Council (EP-SRC) via EP/W005859/1 and EP/Y011805/1.

References

- U. Alon. *An Introduction to Systems Biology: Design Principles of Biological Circuits*. Chapman and Hall/CRC, 2019.
- P. Alquier and M. Gerber. Universal robust regression via maximum mean discrepancy. *Biometrika*, 111(1):71–92, 2024.
- P. Alquier, B.-E. Chérif-Abdellatif, A. Derumigny, and J.-D. Fermanian. Estimation of copulas via maximum mean discrepancy. *Journal of the American Statistical Association*, 118(543):1997–2012, 2023.
- M. Altamirano, F.-X. Briol, and J. Knoblauch. Robust and scalable Bayesian online changepoint detection. In *Proceedings of the 40th International Conference on Machine Learning*, 2023.
- M. Altamirano, F.-X. Briol, and J. Knoblauch. Robust and conjugate Gaussian process regression. In *Proceedings of the 41st International Conference on Machine Learning*, 2024.
- L. Ambrosio, N. Gigli, and G. Savaré. *Gradient flows: In metric spaces and in the space of probability measures*. Springer Science & Business Media, 2008.
- M. A. Beaumont. Approximate Bayesian computation in evolution and ecology. *Annual Review of Ecology, Evolution, and Systematics*, 41(1):379–406, 2010.
- A. Berlinet and C. Thomas-Agnan. *Reproducing Kernel Hilbert Spaces in Probability and Statistics*. Springer Science & Business Media, 2011.
- P. G. Bissiri, C. C. Holmes, and S. G. Walker. A general framework for updating belief distributions. *Journal of the Royal Statistical Society, Series B*, 78(5):1103, 2016.
- F.-X. Briol, A. Barp, A. B. Duncan, and M. Girolami. Statistical inference for generative models with maximum mean discrepancy. *arXiv preprint arXiv:1906.05944*, 2019a.
- F.-X. Briol, C. J. Oates, M. Girolami, M. A. Osborne, and D. Sejdinovic. Probabilistic integration: A role in statistical computation? *Statistical Science*, 34(1):1–22, 2019b.
- Y. Chen, X. Cheng, J. Niles-Weed, and J. Weare. Convergence of unadjusted Langevin in high dimensions: Delocalization of bias. *arXiv preprint arXiv:2408.13115*, 2024.
- B.-E. Chérif-Abdellatif and P. Alquier. MMD-Bayes: Robust Bayesian estimation via maximum mean discrepancy. In *Proceedings of the Symposium on Advances in Approximate Bayesian Inference*. PMLR, 2020.
- B.-E. Chérif-Abdellatif and P. Alquier. Finite sample properties of parametric MMD estimation: Robustness to misspecification and dependence. *Bernoulli*, 28(1):181–213, 2022.
- V. Chernozhukov and H. Hong. An MCMC approach to classical estimation. *Journal of Econometrics*, 115(2):293–346, 2003.
- L. Chizat. Mean-field Langevin dynamics: Exponential convergence and annealing. *Transactions on Machine Learning Research*, 2022.
- K. Chwialkowski, H. Strathmann, and A. Gretton. A kernel test of goodness of fit. In *Proceedings of the 33rd International Conference on Machine Learning*, 2016.
- F. R. Crucinio, V. De Bortoli, A. Doucet, and A. M. Johansen. Solving a class of Fredholm integral equations of the first kind via Wasserstein gradient flows. *Stochastic Processes and Applications*, 173(104374), 2024.
- K. Csilléry, M. G. Blum, O. E. Gaggiotti, and O. François. Approximate Bayesian computation (ABC) in practice. *Trends in Ecology & Evolution*, 25(7):410–418, 2010.
- A. P. Dawid. Probability forecasting. In *Encyclopedia of Statistical Sciences*. Wiley Online Library, 1986.
- C. Dellaporta, J. Knoblauch, T. Damoulas, and F.-X. Briol. Robust Bayesian inference for simulator-based models via the MMD posterior bootstrap. In *Proceedings of the 25th International Conference on Artificial Intelligence and Statistics*, 2022.
- G. Duran-Martin, M. Altamirano, A. Shestopaloff, L. Sánchez-Betancourt, J. Knoblauch, M. Jones, F.-X. Briol, and K. P. Murphy. Outlier-robust Kalman

- filtering through generalised Bayes. In *Proceedings of the 41st International Conference on Machine Learning*, 2024.
- A. O. Durmus and A. Eberle. Asymptotic bias of inexact Markov chain Monte Carlo methods in high dimension. *Annals of Applied Probability*, 34(4):3435–3468, 2024.
- E. Fong, C. Holmes, and S. G. Walker. Martingale posterior distributions. *Journal of the Royal Statistical Society, Series B*, 85(5):1357–1391, 2023.
- D. T. Frazier, J. Knoblauch, and C. Drovandi. The impact of loss estimation on Gibbs measures. *arXiv preprint arXiv:2404.15649*, 2024.
- S. Ghosal and A. van der Vaart. Convergence rates of posterior distributions for non-IID observations. *Annals of Statistics*, 35(1):192–223, 2007.
- S. Ghosal, J. K. Ghosh, and A. W. Van Der Vaart. Convergence rates of posterior distributions. *Annals of Statistics*, 28(2):500–531, 2000.
- A. Ghosh and A. Basu. Robust Bayes estimation using the density power divergence. *Annals of the Institute of Statistical Mathematics*, 68:413–437, 2016.
- J. Gorham and L. Mackey. Measuring sample quality with kernels. In *Proceedings of the 34th International Conference on Machine Learning*, 2017.
- A. Gretton, K. M. Borgwardt, M. J. Rasch, B. Schölkopf, and A. Smola. A kernel two-sample test. *The Journal of Machine Learning Research*, 13(1):723–773, 2012.
- J. Hermans, A. Delaunoy, F. Rozet, A. Wehenkel, and G. Louppe. A crisis in simulation-based inference? Beware, your posterior approximations can be unfaithful. *Transactions on Machine Learning Research*, 2022.
- R. Hilger, M. Scheulen, and D. Strumberg. The Ras-Raf-MEK-ERK pathway in the treatment of cancer. *Oncology Research and Treatment*, 25(6):511–518, 2002.
- G. Hooker and A. N. Vidyashankar. Bayesian model robustness via disparities. *Test*, 23:556–584, 2014.
- K. Hu, Z. Ren, D. Šiška, and L. Szpruch. Mean-field Langevin dynamics and energy landscape of neural networks. *Annales de l’Institut Henri Poincaré, Probabilités et Statistiques*, 57(4):2043–2065, 2021.
- H. Husain and J. Knoblauch. Adversarial interpretation of Bayesian inference. In *Proceedings of the 33rd International Conference on Algorithmic Learning Theory*, 2022.
- M. Jankowiak, G. Pleiss, and J. Gardner. Deep sigma point processes. In *Proceedings of the 36th Conference on Uncertainty in Artificial Intelligence*, 2020a.
- M. Jankowiak, G. Pleiss, and J. Gardner. Parametric Gaussian process regressors. In *Proceedings of the 37th International Conference on Machine Learning*, 2020b.
- C. Jordan-Squire. *Convex Optimization over Probability Measures*. PhD thesis, University of Washington, 2015.
- M. C. Kennedy and A. O’Hagan. Bayesian calibration of computer models. *Journal of the Royal Statistical Society, Series B*, 63(3):425–464, 2001.
- J. Knoblauch, J. E. Jewson, and T. Damoulas. Doubly robust Bayesian inference for non-stationary streaming data with beta-divergences. 2018.
- J. Knoblauch, J. Jewson, and T. Damoulas. An optimization-centric view on Bayes’ rule: Reviewing and generalizing variational inference. *Journal of Machine Learning Research*, 23(132):1–109, 2022.
- A. Kucukelbir, D. Tran, R. Ranganath, A. Gelman, and D. M. Blei. Automatic differentiation variational inference. *Journal of Machine Learning Research*, 18(14):1–45, 2017.
- C. Kwang-Hyun, S. Sung-Young, K. Hyun-Woo, O. Wolkenhauer, B. McFerran, and W. Kolch. Mathematical modeling of the influence of RKIP on the ERK signaling pathway. <https://www.ebi.ac.uk/biomodels/BIOMD0000000647>, 2003a.
- C. Kwang-Hyun, S. Sung-Young, K. Hyun-Woo, O. Wolkenhauer, B. McFerran, and W. Kolch. Mathematical modeling of the influence of RKIP on the ERK signaling pathway. In *Proceedings of the 1st International Conference on Computational Methods in Systems Biology*, 2003b.
- N. Laird. Nonparametric maximum likelihood estimation of a mixing distribution. *Journal of the American Statistical Association*, 73(364):805–811, 1978.
- Y. Li and Y. Gal. Dropout inference in Bayesian neural networks with alpha-divergences. In *Proceedings of the 34th International Conference on Machine Learning*, 2017.
- B. G. Lindsay. *Mixture Models: Theory, Geometry, and Applications*. Institute of Mathematical Statistics, 1995.
- Q. Liu, J. Lee, and M. Jordan. A kernelized Stein discrepancy for goodness-of-fit tests. In *Proceedings of the 33rd International Conference on Machine Learning*, 2016.
- R. S. Malik-Sheriff, M. Glont, T. V. N. Nguyen, K. Tiwari, M. G. Roberts, A. Xavier, M. T. Vu, J. Men, M. Maire, S. Kananathan, E. L. Fairbanks, J. P. Meyer, C. Arankalle, T. M. Varusai, V. Knight-Schrijver, L. Li, C. Dueñas-Roca,

- G. Dass, S. M. Keating, Y. M. Park, N. Buso, N. Rodriguez, M. Hucka, and H. Hermjakob. BioModels — 15 years of sharing computational models in life science. *Nucleic Acids Research*, 48(D1):D407–D415, 2020.
- A. Masegosa. Learning under model misspecification: Applications to variational and ensemble methods. 2020.
- T. Matsubara, J. Knoblauch, F.-X. Briol, and C. J. Oates. Robust generalised Bayesian inference for intractable likelihoods. *Journal of the Royal Statistical Society, Series B*, 84(3):997–1022, 2022.
- T. Matsubara, J. Knoblauch, F.-X. Briol, and C. J. Oates. Generalized Bayesian inference for discrete intractable likelihood. *Journal of the American Statistical Association*, 119:2345–2355, 2024.
- Y. McLatchie, E. Fong, D. T. Frazier, and J. Knoblauch. Predictive performance of power posteriors. *arXiv preprint arXiv:2408.08806*, 2024.
- J. W. Miller. Asymptotic normality, concentration, and coverage of generalized posteriors. *Journal of Machine Learning Research*, 22(1):7598–7650, 2021.
- W. R. Morningstar, A. Alemi, and J. V. Dillon. PACm-Bayes: Narrowing the empirical risk gap in the misspecified Bayesian regime. In *Proceedings of the 25th International Conference on Artificial Intelligence and Statistics*, 2022.
- A. Nitanda, D. Wu, and T. Suzuki. Convex analysis of the mean field Langevin dynamics. In *Proceedings of the 25th International Conference on Artificial Intelligence and Statistics*, 2022.
- C. J. Oates, B. T. Hennessy, Y. Lu, G. B. Mills, and S. Mukherjee. Network inference using steady-state data and Goldbeter–Koshland kinetics. *Bioinformatics*, 28(18):2342–2348, 2012.
- C. J. Oates, M. Girolami, and N. Chopin. Control functionals for Monte Carlo integration. *Journal of the Royal Statistical Society, Series B*, 79(3):695–718, 2017.
- R. Ranganath, S. Gerrish, and D. Blei. Black box variational inference. In *Proceedings of the 17th International Conference on Artificial Intelligence and Statistics*, 2014.
- G. O. Roberts and R. L. Tweedie. Exponential convergence of Langevin distributions and their discrete approximations. *Bernoulli*, 2(4):341–363, 1996.
- S. M. Schmon, P. W. Cannon, and J. Knoblauch. Generalized posteriors in approximate Bayesian computation. In *Proceedings of the 3rd Symposium on Advances in Approximate Bayesian Inference*, 2020.
- R. Sheth and R. Khardon. Pseudo-Bayesian learning via direct loss minimization with applications to sparse Gaussian process models. In *Proceedings of the 6th Symposium on Advances in Approximate Bayesian Inference*, 2020.
- B. K. Sriperumbudur, K. Fukumizu, and G. R. Lanckriet. Universality, characteristic kernels and RKHS embedding of measures. *Journal of Machine Learning Research*, 12(7), 2011.
- A. W. Van der Vaart. *Asymptotic Statistics*. Cambridge University Press, 2000.
- C. Villacampa-Calvo and D. Hernandez-Lobato. Alpha divergence minimization in multi-class Gaussian process classification. *Neurocomputing*, 378: 210–227, 2020.
- S. G. Walker. Bayesian inference with misspecified models. *Journal of Statistical Planning and Inference*, 143(10):1621–1633, 2013.
- D. Wang, S. A. Boerner, J. D. Winkler, and P. M. LoRusso. Clinical experience of MEK inhibitors in cancer therapy. *Biochimica et Biophysica Acta (BBA)-Molecular Cell Research*, 1773(8): 1248–1255, 2007.
- V. D. Wild, S. Ghalebikesabi, D. Sejdinovic, and J. Knoblauch. A rigorous link between deep ensembles and (variational) Bayesian methods. In *Proceedings of the 36th Conference on Neural Information Processing Systems*, 2023.
- P.-S. Wu and R. Martin. A comparison of learning rate selection methods in generalized Bayesian inference. *Bayesian Analysis*, 18(1):105–132, 2023.
- K. Yeung, P. Janosch, B. McFerran, D. W. Rose, H. Mischak, J. M. Sedivy, and W. Kolch. Mechanism of suppression of the Raf/MEK/extracellular signal-regulated kinase pathway by the Raf kinase inhibitor protein. *Molecular and Cellular Biology*, 20(9):3079–3085, 2000.

Supplement

These appendices accompany the manuscript *Prediction-Centric Uncertainty Quantification*.

A Existence, Uniqueness, and Characterisation of Q_n

This appendix presents sufficient conditions for the existence and uniqueness of a minimiser Q_n of (2), and an implicit characterisation of Q_n which in turn suggests some alternative sampling strategies that could be used (c.f. Appendix C).

First, we establish sufficient conditions for existence and uniqueness of Q_n , which are stated in Theorem 1. These leverage the convexity of (7), which follows from entropic regularisation; i.e. from the use of KL as the regulariser in (2).

Theorem 1 (Existence and Uniqueness of Q_n). *Assume that $\Theta = \mathbb{R}^p$, $p \in \mathbb{N}$, and that:*

1. $k : \mathcal{X} \times \mathcal{X} \rightarrow \mathbb{R}$ is bounded
2. Q_0 has density $q_0 \propto \exp(-U_0)$ where ∇U_0 is Lipschitz and satisfies a coercivity condition $\langle \theta, \nabla U_0(\theta) \rangle \geq c \cdot \|\theta\|^2 - c'$ for some $c > 0, c' \in \mathbb{R}$, and all $\theta \in \Theta$.

Then Q_n exists and is unique for all $\lambda_n > 0$.

Proof of Theorem 2. The result is essentially that of Proposition 2.5 of Hu et al. [2021]; here for the reader we provide the high-level argument. The starting point is to recall that Q_n minimises (2); i.e. Q_n minimises

$$\mathcal{F}_n(Q) := \frac{1}{2} \text{MMD}^2(P_n, P_Q) + \text{KL}(Q, Q_0)$$

Since we have assumed that our kernel k is bounded, it follows that the MMD term is also bounded. It hence follows that \mathcal{F}_n is finite whenever $\text{KL}(Q, Q_0)$ is finite, i.e. the domain of \mathcal{F}_n is the domain of $\text{KL}(\cdot, Q_0)$. It is well-known that this functional is strictly convex on its convex domain, and bounded below by 0. Additionally, for any Mercer kernel k , the functional MMD^2 is always convex (classically, rather than geodesically), and the mapping $Q \mapsto P_Q$ is linear, implying that the composite mapping $Q \mapsto \text{MMD}^2(P_n, P_Q)$ is also convex and lower-bounded. It hence follows that \mathcal{F}_n is strictly convex on its convex domain, and is lower-bounded. Existence of a minimiser holds by routine arguments involving lower semi-continuity of the objective, see e.g. Appendix A of Wild et al. [2023], and strict convexity implies uniqueness. \square

The second result we present is an implicit characterisation for Q_n itself, in Theorem 2. This is obtained by setting to zero the Wasserstein gradient $\nabla_W \mathcal{F}_n(Q)$.

Theorem 2 (Characterisation of Q_n). *Under the same conditions as Theorem 1, Q_n satisfies the implicit equation*

$$Q_n(d\theta) = \frac{1}{Z} \cdot Q_0(d\theta) \cdot \exp\left(-\frac{1}{\lambda_n} \cdot V_{Q_n}(\theta)\right) \quad (13)$$

where, letting $\kappa_0(\theta, \vartheta) = \langle \mu_k(P_\theta), \mu_k(P_\vartheta) \rangle_{\mathcal{H}(k)}$,

$$V_{Q_n}(\theta) = \int \kappa_0(\theta, \cdot) dQ_n - \langle \mu_k(P_n), \mu_k(P_\theta) \rangle_{\mathcal{H}(k)},$$

and where $Z > 0$ is a normalisation constant.

Proof. Using the expression for the Stein kernel κ_{P_n} in (6), and the fact that Q is a probability measure, we can write the entropy-regularised free energy (7) as

$$\begin{aligned} \mathcal{F}_n(Q) = \frac{1}{2} \left\{ \frac{1}{n^2} \sum_{i=1}^n \sum_{j=1}^n k(y_i, y_j) - \frac{2}{n} \sum_{i=1}^n \iint k(y_i, y) dP_\theta(y) dQ(\theta) \right. \\ \left. + \iiint k(y, y') dP_\theta(y) dP_\vartheta(y') dQ(\theta) dQ(\vartheta) \right\} + \lambda_n \int \log\left(\frac{dQ}{dQ_0}(\theta)\right) dQ(\theta) \end{aligned}$$

Taking the functional derivative with respect to Q , we obtain that

$$\delta\mathcal{F}_n(Q)(\theta) = -\underbrace{\frac{1}{n} \sum_{i=1}^n \int k(y_i, y) \, dP_\theta(y) + \iiint k(y, y') \, dP_\theta(y) dP_\theta(y') \, dQ(\vartheta)}_{=V_{Q_n}(\theta)} + \lambda_n \left[1 + \log \left(\frac{dQ}{dQ_0}(\theta) \right) \right].$$

The minimiser $Q = Q_n$ of the free energy satisfies $\delta\mathcal{F}_n(\theta) = \text{constant}$ (where the constant term can be seen as a Lagrange multiplier reflecting the constraint that Q_n be a probability measure), leading to the implicit equation

$$0 = V_{Q_n}(\theta) + \lambda_n \log \left(\frac{dQ}{dQ_0}(\theta) \right) + \text{constant},$$

and upon rearranging we obtain

$$\frac{dQ}{dQ_0}(\theta) \propto \exp \left(-\frac{1}{\lambda_n} V_{Q_n}(\theta) \right),$$

which is equivalent to the stated result. \square

While the regularising effect of Q_0 is well-understood for Gibbs measures like Q_n^\dagger [Bissiri et al., 2016, Knoblauch et al., 2022], it is perhaps surprising that Q_0 acts on Q_n in essentially the same way in PCUQ, as shown in (13). This implicit characterisation of Q_n is also interesting in that it suggests alternative sampling strategies, which are discussed in Appendix C.

B Computing the Stein Kernel κ_{P_n} and its Gradient $\nabla_1 \kappa_{P_n}$

This appendix is devoted to discussion of different computational strategies to computing integrals that appear in both the Stein kernel κ_{P_n} and its gradient $\nabla_1 \kappa_{P_n}$. The case of independent data is discussed in Appendix B.1, while the case of dependent data is discussed in Appendix B.2. In addition, we highlight that a reduction in computational complexity is possible for dependent data in the regime $\ell_{\mathcal{X}} \rightarrow 0$ in Appendix B.3.

B.1 Independent Data

Simulation of (9) requires the gradient $\nabla_1 \kappa_{P_n}$ of the Stein kernel. Several techniques are available to compute the gradient (with respect to θ) of the integrals appearing in expression (6) for the Stein kernel. For simplicity we focus on the case of integrals with respect to P_θ , but double integrals with respect to P_θ can be similarly handled.

Analytic Case For particular combinations of k and P_θ the integrals appearing in (6) will be computable in closed form and derivatives of the kernel κ_{P_n} may be exactly computed. This scenario occurs, for example, when k is a Gaussian kernel and P_θ is a Gaussian distribution; other scenarios where the kernel mean embedding can be exactly computed are listed in Table 1 of Briol et al. [2019b].

Score Gradient Case In the case where P_θ admits a positive and differentiable pdf $p_\theta(\cdot)$, under regularity conditions we can calculate that

$$\nabla_\theta \int k(y_i, y) \, dP_\theta(y) = \nabla_\theta \int k(y_i, y) p_\theta(y) \, dy = \int k(y_i, y) \nabla_\theta p_\theta(y) \, dy = \int k(y_i, y) (\nabla_\theta \log p_\theta(y)) \, dP_\theta(y) \quad (14)$$

and obtain a natural approximation using Monte Carlo. This is analogous to how gradients are calculated in *black-box variational inference* [Ranganath et al., 2014].

Reparametrisation Trick If we can express $P_\theta = \text{law}(f_\theta(U))$ for some θ -independent random variable $U \sim \mathcal{U}$ then we can employ the *reparametrisation trick* to express

$$\nabla_\theta \int k(y_i, y) \, dP_\theta(y) = \nabla_\theta \int k(y_i, f_\theta(u)) \, d\mathcal{U}(u) = \int \nabla_\theta f_\theta(u) \nabla_2 k(y_i, f_\theta(u)) \, d\mathcal{U}(u)$$

and obtain a natural approximation using Monte Carlo. This is analogous to how gradients are calculated in *automatic differentiation variational inference* [Kucukelbir et al., 2017].

B.2 Dependent Data

The strategies for computing the gradient $\nabla_1 \kappa_{P_n}$ that were presented in Appendix B.1 for the setting where data are independent can be extended to the regression setting considered in Section 5.4, where data are dependent.

Analytic Case The Stein kernel is now

$$\begin{aligned} \kappa_{P_n}(\theta, \vartheta) = & \frac{1}{n^2} \sum_{i,j=1}^n k((x_i, y_i), (x_j, y_j)) - \frac{1}{n^2} \sum_{i,j=1}^n \int k((x_i, y_i), (x_j, y)) dP_\theta(y|x_j) \\ & - \frac{1}{n^2} \sum_{i,j=1}^n \int k((x_i, y_i), (x_j, y)) dP_\vartheta(y|x_j) + \frac{1}{n^2} \sum_{i,j=1}^n \iint k((x_i, y), (x_j, y')) dP_\theta(y|x_i) dP_\vartheta(y'|x_j). \end{aligned} \quad (15)$$

The case where $k : (\mathcal{X} \times \mathcal{Y}) \times (\mathcal{X} \times \mathcal{Y}) \rightarrow \mathbb{R}$ is a separable Gaussian kernel and $P_\theta(\cdot|x)$ is a Gaussian measurement error model can be calculated in closed form, and we present this calculation in Appendix D. This was the computational approach used to perform all experiments in Section 6.

Score Gradient Case The score gradient approach can be immediately extended to the dependent data setting via

$$\begin{aligned} \nabla_\theta \int k((x_i, y_i), (x, y)) d\bar{P}_\theta(x, y) &= \nabla_\theta \left\{ \frac{1}{n} \sum_{j=1}^n \int k((x_i, y_i), (x_j, y)) dP_\theta(y|x_j) \right\} \\ &= \frac{1}{n} \sum_{j=1}^n \int k((x_i, y_i), (x_j, y)) (\nabla_\theta \log p_\theta(y|x_j)) dP_\theta(y|x_j). \end{aligned} \quad (16)$$

Reparametrisation Trick For the reparametrisation trick we now require a map f_θ such that $y_i|x_i$ is modelled as $f_\theta(U, x)$ where $U \sim \mathcal{U}$. The gradient that we seek is then

$$\begin{aligned} \nabla_\theta \int k((x_i, y_i), (x, y)) d\bar{P}_\theta(x, y) &= \nabla_\theta \left\{ \frac{1}{n} \sum_{j=1}^n \int k((x_i, y_i), (x_j, f_\theta(u, x_j))) d\mathcal{U}(u) \right\} \\ &= \frac{1}{n} \sum_{j=1}^n \int \nabla_\theta f_\theta(u, x_j) \nabla_{2,2} k((x_i, y_i), (x_j, f_\theta(u, x_j))) d\mathcal{U}(u) \end{aligned}$$

where $\nabla_{2,2} k((a, b), (c, d))$ denotes the gradient with respect to argument d .

B.3 Dependent Data; Simplification when $\ell_{\mathcal{X}} \rightarrow 0$

In the dependent data setting, evaluation of the Stein kernel κ_{P_n} in (15) incurs a computational cost of $O(n^2)$ in general, as opposed to the $O(n)$ cost of computing (6) when data are independent. Fortunately we can simultaneously recover the $O(n)$ cost while also mitigating negative effects of the lifting in Section 5.4 by considering the (x, x') dependence of the kernel $k((x, y), (x', y'))$ in a particular objective limit. This follows an identical strategy proposed in Section 3.4 of Alquier and Gerber [2024].

For the experiments that we report in the main text we used the Gaussian kernel where $\ell_{\mathcal{X}}$ is the bandwidth describing the similarity between two distinct covariates x and x' . A natural limit exists when $\ell_{\mathcal{X}} \rightarrow 0$, where upon the kernel $k : (\mathcal{X} \times \mathcal{Y}) \times (\mathcal{X} \times \mathcal{Y}) \rightarrow \mathbb{R}$ becomes

$$k((x, y), (x', y')) = \exp \left(-\frac{\|x - x'\|^2}{\ell_{\mathcal{X}}^2} - \frac{\|y - y'\|^2}{\ell_{\mathcal{Y}}^2} \right) \rightarrow \begin{cases} k(y, y') := \exp \left(-\frac{\|y - y'\|^2}{\ell_{\mathcal{Y}}^2} \right) & \text{if } x = x' \\ 0 & \text{if } x \neq x' \end{cases} \quad (17)$$

and upon plugging this limiting expression into (15) we obtain

$$\begin{aligned} \kappa_{P_n}(\theta, \vartheta) = & \frac{1}{n^2} \sum_{i=1}^n k(y_i, y_i) - \frac{1}{n^2} \sum_{i=1}^n \int k(y_i, y) \, dP_\theta(y|x_i) \\ & - \frac{1}{n^2} \sum_{i=1}^n \int k(y_i, y) \, dP_\vartheta(y|x_i) + \frac{1}{n^2} \sum_{i=1}^n \iint k(y, y') \, dP_\theta(y|x_i) dP_\vartheta(y'|x_i), \end{aligned}$$

which is seen to have computational cost $O(n)$. In addition to reducing cost, this limit has the effect that *only* data y_i corresponding to precisely the covariate x_i are used to assess the performance of the model $P_\theta(dy|x_i)$, mitigating negative effects of the lifting that we described in Section 5.4.

C Alternative Sampling Methods for Q_n

The aim of this appendix is to comment on the possibility of alternative sampling strategies for Q_n . From (9), one can verify by inspection that $\{\theta_t\}_{1:N} = (\theta_t^1, \dots, \theta_t^N)$ is precisely the Langevin diffusion with joint target distribution

$$\tilde{Q}_n^{\otimes N}(\{d\theta\}_{1:N}) \propto \left(\prod_{i=1}^N Q_0(d\theta^i) \right) \cdot \exp \left(-\frac{1}{\lambda_n} \cdot \frac{1}{N-1} \sum_{1 \leq i < j \leq N} \kappa_{P_n}(\theta^i, \theta^j) \right) \quad (18)$$

Following this observation, one could consider using a general *Markov chain Monte Carlo* (MCMC) sampler to generate approximate samples from (18); at stationarity, each of the N components of the Markov chain would then represent an approximate sample from Q_n . Of course, for large N the dimension of the state space Θ^N can be expected to create difficulties for efficient MCMC schemes which exactly preserve the target measure. Nevertheless, for approximate algorithms such as the unadjusted Langevin algorithm, implementation remains feasible, and there are even suggestions [Durmus and Eberle, 2024, Chen et al., 2024] that the asymptotic bias remains well-behaved in this limit; we highlight this as a direction for future work.

Comparing the above with $Q_n^{\otimes N}(\{\theta\}_{1:N}) := \prod_{i=1}^N Q_n(\theta^i)$, the joint density of N independent draws from Q_n (13), we observe that $\tilde{Q}_n^{\otimes N}$ (18) differs in that the implicit term $\int \kappa_0(\theta, \cdot) dQ_n$ is replaced by an explicit term $\frac{1}{N-1} \sum_{j \neq i} \kappa_0(\theta^i, \theta^j)$. This is essentially the key ingredient of mean-field Langevin dynamics; see e.g. Chizat [2022], Hu et al. [2021], Nitanda et al. [2022].

D Calculations for Gaussian Measurement Models

This appendix contains explicit calculations for the integral terms appearing in the Stein kernel κ_{P_n} and its gradient $\nabla_1 \kappa_{P_n}$ for the Gaussian measurement error model $P_\theta(\cdot|x) = \mathcal{N}(w_\theta(x), \sigma^2 I_{p \times p})$, which is extremely common in scientific modelling. For analytic tractability we consider a separable Gaussian kernel

$$k((x, y), (x', y')) = \exp \left(-\frac{\|x - x'\|^2}{2\ell_x^2} \right) \exp \left(-\frac{\|y - y'\|^2}{2\ell_y^2} \right)$$

so that we can analytically evaluate the integrals

$$\begin{aligned} \int \exp \left(-\frac{\|y_i - y\|^2}{2\ell_y^2} \right) \, dP_\theta(y|x_j) &= \left(\frac{\ell_y^2}{\ell_y^2 + \sigma^2} \right)^{p/2} \exp \left(-\frac{\|y_i - w_\theta(x_j)\|^2}{2(\ell_y^2 + \sigma^2)} \right) \\ \iint \exp \left(-\frac{\|y - y'\|^2}{2\ell_y^2} \right) \, dP_\theta(y|x_i) dP_\vartheta(y'|x_j) &= \left(\frac{\ell_y^2}{\ell_y^2 + 2\sigma^2} \right)^{p/2} \exp \left(-\frac{\|w_\theta(x_i) - w_\vartheta(x_j)\|^2}{2(\ell_y^2 + 2\sigma^2)} \right) \end{aligned}$$

and explicitly differentiate these with respect to θ to obtain

$$\begin{aligned} \nabla_{\theta} \int \exp\left(-\frac{\|y_i - y\|^2}{2\ell_y^2}\right) dP_{\theta}(y|x_j) &= \frac{1}{\ell_y^2} \left(\frac{\ell_y^2}{\ell_y^2 + \sigma^2}\right)^{p/2+1} \\ &\quad \times \exp\left(-\frac{\|y_i - w_{\theta}(x_j)\|^2}{2(\ell_y^2 + \sigma^2)}\right) [\nabla_{\theta} w_{\theta}(x_j)][y_i - w_{\theta}(x_j)] \\ \nabla_{\theta} \iint \exp\left(-\frac{\|y - y'\|^2}{2\ell_y^2}\right) dP_{\theta}(y|x_i) dP_{\theta}(y'|x_j) &= \frac{1}{\ell_y^2} \left(\frac{\ell_y^2}{\ell_y^2 + 2\sigma^2}\right)^{p/2+1} \\ &\quad \times \exp\left(-\frac{\|w_{\theta}(x_i) - w_{\theta}(x_j)\|^2}{2(\ell_y^2 + 2\sigma^2)}\right) [-\nabla_{\theta} w_{\theta}(x_i)][w_{\theta}(x_i) - w_{\theta}(x_j)]. \end{aligned}$$

E Additional Empirical Details

This appendix contains all details needed to reproduce the empirical results that we report in Section 6. Details for the LVM experiment are contained in Appendix E.1, while details for the cell signalling experiment are contained in Appendix E.2.

E.1 Lotka–Volterra Model

Parameter Settings The data-generating parameters that we used for the LVM were: $\alpha = \text{logit}^{-1}(-2)$, $\beta = \text{logit}^{-1}(-4)$, $\gamma = 0.4$, $\delta = 0.02$. The initial prey and predator concentrations were $\xi_1 = 10$ and $\xi_2 = 10$. The SDE model described in Section 6.1 with intrinsic noise $\epsilon_1 = 0$, $\epsilon_2 = 0.4$ was discretised for numerical simulation using the reversible Heun’s method with time step $dx = 0.01$, and simulated from $x = 0$ to $x = 60$. Data were extracted at times $x_{1:n}$ ranging from 0 to 60 in increments of 1.0, with Gaussian measurement noise of variance $\sigma^2 = 1$ added.

MMD-Bayes The MMD-Bayes method of Chérif-Abdellatif and Alquier [2020] is an instance of generalised variational inference whose output distribution Q is given by the Radon–Nikodym derivative

$$\frac{dQ}{dQ_0}(\theta) = \exp(-\beta \text{MMD}^2(P_n, P_{\theta}))$$

where $\beta > 0$ was termed a *learning rate*. For our implementation of MMD-Bayes we used the same kernel k to construct the MMD as was used for PCUQ, and we employed the same learning rate $\beta = \exp(np)$ as used in Chérif-Abdellatif and Alquier [2020] where $\theta \in \mathbb{R}^p$ ($p = 2$ for the LVM).

Convergence of Sampling Methods The standard Bayesian posterior and the MMD-Bayes output were each numerically approximated using 10 parallel instances of the *Metropolis-adjusted Langevin algorithm* (MALA) [Roberts and Tweedie, 1996], initialised from the true parameter values (i.e. to ensure a warm start). A total of 5000 iterations were performed, with the proposal variance parameter tuned to avoid pathological behaviour, and only the remaining third of the samples were retained. The PCUQ output was obtained using MALA on the joint distribution of 10 particles, together with the warm start with the same number of iterations. Trace plots, demonstrating convergence of the sampling algorithms, are displayed in Figure 3.

Insensitivity to λ_{\star} The proposed PCUQ method involves a regularisation parameter λ_n , and in the main text we proposed a heuristic choice $\lambda_n = \lambda_{\star}$. To assess the sensitivity to this choice, we re-computed predictive distributions based on alternative values of λ_n , presenting the results in Figure 4. These results demonstrate that predictive performance is rather insensitive to reducing the size of λ_n (of course, for very large λ_n we will recover Q_0). This may be explained by the fact that predictive uncertainty is driven mainly by the data in PCUQ, with the role of the distribution Q_0 being limited to convexification of the gradient flow objective in Equation (2), and for this purpose a relatively small value of λ_n is sufficient.

Insensitivity to N The proposed gradient flow algorithm involves selecting a number of particles N , and in the main text we presented results based on $N = 10$. To assess the sensitivity to this choice, we re-computed

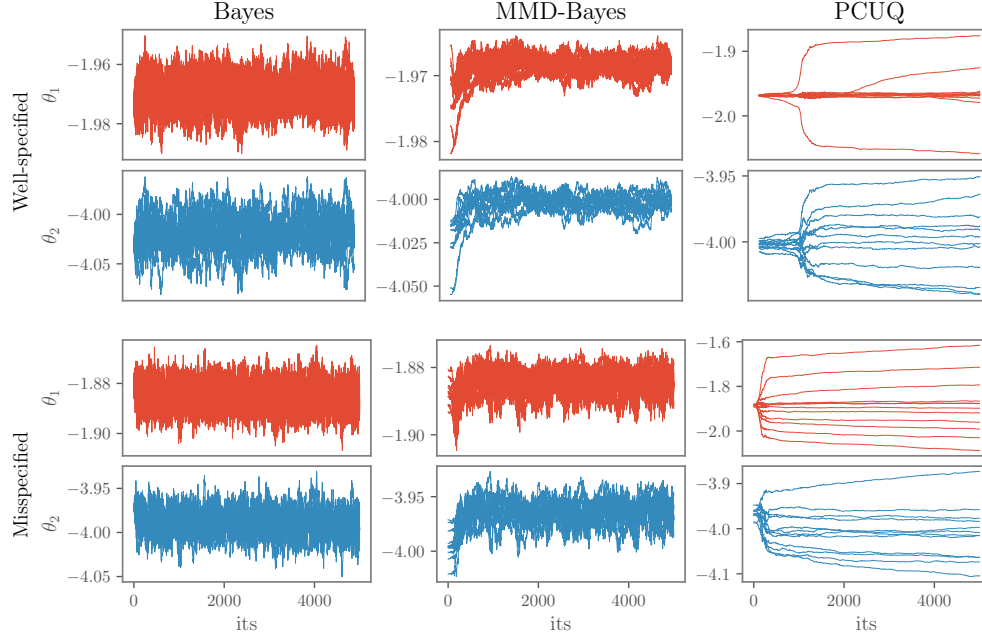


Figure 3: Lotka–Volterra model: Convergence of sampling algorithms. Here trace plots for θ_1 (red) and θ_2 (blue) are presented for the sampling algorithms used to approximate the standard Bayesian posterior (left), the MMD-Bayes output (middle) and the proposed PCUQ method (right). The top row corresponds to the well-specified case where data were generated from the ODE model, while the bottom row corresponds to the misspecified case where data were generated from the SDE model.

trace plots based on alternative choices of N in Figures 5 and 6. A greater number of particles provides a more accurate spatial discretisation on the right hand side of (9), as well as better expressive flexibility of characterising uncertainty. In the well-specified case (Figure 5), we see that the number of particles affects the discretisation of Q^t when the number of particles is low. In the misspecified case (Figure 6), we see that despite the increasing number of particles, the overall span of the particle distribution remains unchanged. Therefore, the outcome of PCUQ remains insensitive to the number of particles when the discretization and expressivity are adequately addressed.

Dependence on Parameter Settings In response to a reviewer who asked about the sensitivity of these results to the specific parameter settings, we repeated the LVM experiment with the alternative parameter settings $\alpha = \text{logit}^{-1}(-1)$, $\beta = \text{logit}^{-1}(-3)$, $\gamma = 0.4$, $\delta = 0.02$. The initial prey and predator concentrations this time were $\xi_1 = 10$ and $\xi_2 = 15$. The SDE model described in Section 6.1 was employed with intrinsic noise $\epsilon_1 = 0.1$, $\epsilon_2 = 0.2$. The corresponding analogue of Figure 1 for these alternative parameter settings is shown as Figure 7. Likewise Figures 8 to 10 are the analogues of Figures 3, 5 and 6.

E.2 Cell Signalling

ERK Signalling Model The ERK pathway is a chain of proteins in mammalian cells that communicates a signal from a receptor on the surface of the cell to the DNA in the nucleus of the cell (see the top panel of Figure 2). In many cancers (e.g. breast, melanoma), a defect in the ERK pathway leads to uncontrolled growth, and as such this pathway has been the subject of considerable research effort. This has included the development of detailed mathematical models of ERK signalling, and the development of compounds that can inhibit steps in the ERK pathway, providing one route to treatment [Hilger et al., 2002].

For the purposes of this case study, we considered one such mathematical model for ERK signalling based on a system of coupled ODEs, due to Kwang-Hyun et al. [2003b]. This model [Kwang-Hyun et al., 2003a], which considers just a subset of the species depicted in Figure 2, was downloaded from the BioModels repository [Malik-Sheriff et al., 2020] on 4 September 2024. It is well-known that protein signalling in mammalian cells

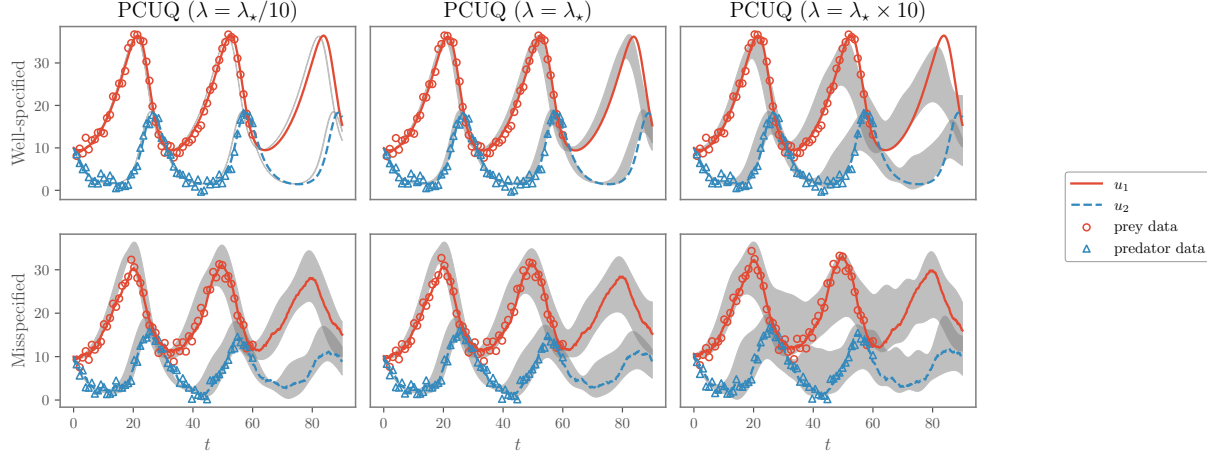


Figure 4: Lotka–Volterra Model: Investigating sensitivity to the regularisation hyperparameter λ_* . The proposed PCUQ method involves a regularisation parameter λ_n , and in the main text we proposed a heuristic choice $\lambda_n = \lambda_*$. To assess the sensitivity to this choice, we re-computed predictive distributions based on the alternative choices $\lambda_n = \lambda_*/10$ (left) and $\lambda_n = \lambda_* \times 10$ (right). It was observed that predictions were almost unchanged in both the well-specified and misspecified context.

is intrinsically stochastic due to finite molecular counts and the spatially heterogeneous, compartmentalised, dynamic cellular environment. This is in contrast to the high copy numbers and spatially homogeneous (“well mixed”) environment that are implicitly assumed in an ODE model [Oates et al., 2012]. Yet, deterministic models are prevalent in Systems Biology, in part due to the valuable use of ODEs as a communicative and logico-deductive tool. There is therefore a real need for statistical techniques that can exploit the rich expert knowledge encoded in an ODE model whilst acknowledging that such an ODE model does not necessarily meet the criteria that we would expect from a statistical model; i.e. an ODE + noise model it is likely to be substantially misspecified.

The model of ERK signalling that we consider takes the form of a coupled system of 11 differential equations, which we write as $du/dx = f(u; \beta)$, representing the evolution of concentrations of the 11 molecular species shown in Table 1. The full system of ODEs is displayed in Figure 11, and contains a total of 11 non-negative rate parameters $\beta = (\beta_1, \dots, \beta_{11})$ that collectively determine the signalling dynamics, together with the initial conditions in the right hand column of Table 1. Here we consider noisy observations $y_{1:n}$ of the concentrations u at times $x_{1:n}$, where the noise follows an additive Gaussian measurement error model (12). This case study is intended to represent the situation where patient- or cell line-specific kinetic parameters are to be inferred from time-course proteomic data; a fundamentally important scientific task [e.g. as considered by the authors Kwang-Hyun et al., 2003b, who developed this model].

Variable Name	Protein/Protein Complex	Initial Concentration
u_1	[Raf1]	2
u_2	[RKIP]	2.5
u_3	[Raf1_RKIP]	0
u_4	[Raf1_RKIP_ERKPP]	0
u_5	[ERK]	0
u_6	[RKIPP]	0
u_7	[MEKPP]	2.5
u_8	[MEKPP_ERK]	0
u_9	[ERKPP]	2.5
u_{10}	[RP]	3
u_{11}	[RKIPP_RP]	0

Table 1: Protein species in the ERK signalling model of [Kwang-Hyun et al., 2003a].

Parameter Settings The data-generating parameters that we used for the ERK model were: $\beta_1 = 0.53$, $\beta_2 = 0.0072$, $\beta_3 = 0.625$, $\beta_4 = 0.00245$, $\beta_5 = 0.0315$, $\beta_6 = 0.8$, $\beta_7 = 0.0075$, $\beta_8 = 0.071$, $\beta_9 = 0.92$, $\beta_{10} = 0.00122$,

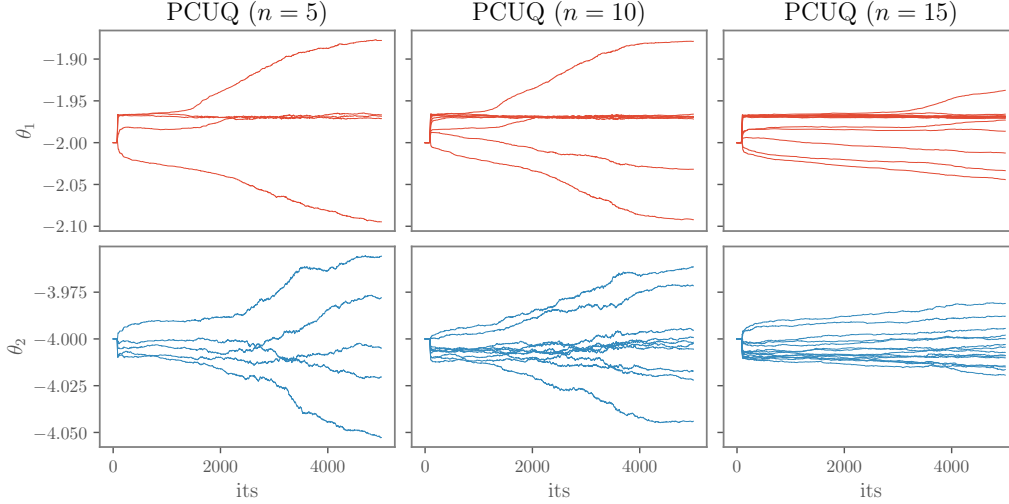


Figure 5: Lotka–Volterra Model: Investigating sensitivity to the number of particles N . The proposed gradient flow algorithm involves selecting a number of particles N , and in the main text we presented results based on $N = 10$. To assess the sensitivity to this choice, we re-computed trace plots based on the alternative choices $N = 5$ (left) and $N = 15$ (right). Here data were generated from the well-specified model.

$\beta_{11} = 0.87$, taken from Kwang-Hyun et al. [2003a]. Similarly to Section 6.1 we work with transformed parameters $\theta_i = \text{logit}(\beta_i)$ so that the sign of the θ_i is unconstrained. The distribution Q_0 (i.e. the prior in the standard Bayesian context) was again taken to be standard multivariate normal.

Data Generation The true molecular concentrations $u(x)$ were simulated from the same model, but where the propensity for molecular interaction was no longer constant but slightly time-varying, reflecting the complexity of the cellular environment in which signalling occurs [Oates et al., 2012]. Specifically, we simulated data based on the ODE model

$$\frac{du}{dx} = f(u; \beta(x))$$

with $\beta_i(x) = (1 + 1/2 \sin(2\pi x/45)) \beta_i$ simulated from $x = 0$ to $x = 60$. Data were extracted at times $x_{1:80}$ ranging from 0 to 45 in increments of $dx = 0.57$, with Gaussian measurement noise of variance $\sigma_i^2 = 0.01\hat{\sigma}_i^2$ added, where $\hat{\sigma}_i$ is a measure of the characteristic scale for the i th molecular concentration, defined as the standard deviation of $u_i(X)$ for a time X sampled from $\text{Uniform}(0, 60)$.

Causal Prediction Task One targeted treatment for cancer sub-types characterised by dysregulated ERK signalling is a *mitogen-activated protein kinase kinase* (MEK) inhibitor compound. A *MEK inhibitor* (MEKi) is a small molecule which is absorbed by the cancer cell and binds to the MEK protein, negatively affecting its kinase functionality. As such, MEKis have been considered as a potential cancer treatment (e.g. of melanoma) [Wang et al., 2007], and examples of MEKis include the drugs *Trametinib*, *Binimetinib*, and *Cobimetinib*. The prediction task that we considered here was to predict the evolution of molecular concentrations – and in particular ERK – under the action of a MEKi treatment. This is a causal prediction task, since we only have data from the regime where the MEKi was not used, and we aim to leverage the explicitly causal ODE model to reason about the effect of the treatment. Concretely, we replace β_6 with $\gamma\beta_6$ on the right hand side of (11) (i.e. an effective reduction in the concentration of the functionally active phosphorylated form of MEK) to obtain the causal model corresponding to the drug-treated cell. Here we fixed $\gamma = 0.01$ (as opposed to setting γ exactly to 0) to acknowledge the limited efficacy of a MEK inhibitor treatment. A key goal is to predict the concentration of ERK (i.e. u_5) and related protein complexes following treatment; this is a natural functional endpoint, since activated ERK translocates to the cell nucleus and regulate gene expression via the phosphorylation of transcription factors [Yeung et al., 2000].

Full results from standard Bayesian inference are shown in Figure 12. Full results from PCUQ are shown in Figure 13. All setting for PCUQ were identical to those used in Section 6.1.

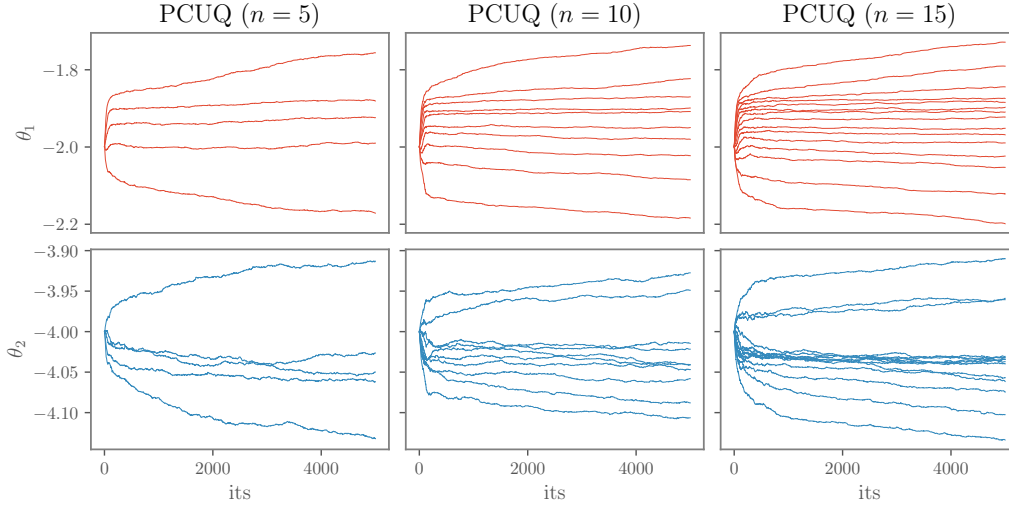


Figure 6: Lotka–Volterra Model: Investigating sensitivity to the number of particles N . The proposed gradient flow algorithm involves selecting a number of particles N , and in the main text we presented results based on $N = 10$. To assess the sensitivity to this choice, we re-computed trace plots based on the alternative choices $N = 5$ (left) and $N = 15$ (right). Here data were generated from the misspecified model.

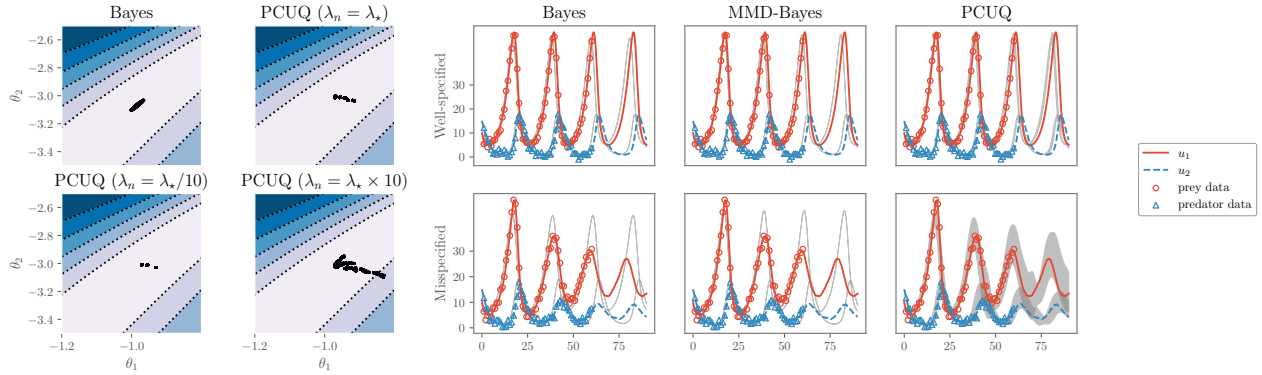


Figure 7: Lotka–Volterra model (alternative parameter settings). Left: Contour plots depict the standard Bayesian posterior, superimposed with samples from the standard Bayesian posterior (Bayes) and the proposed method (PCUQ) with varying regularisation parameter λ_n . Right: Predictive distributions in both the well-specified (top) and misspecified (bottom) context. (Lines depict true prey and predator populations, while the shaded regions depict the predictive quartiles for standard Bayesian inference, the MMD-Bayes method of Chérif-Abdellatif and Alquier [2020], and the proposed PCUQ.)

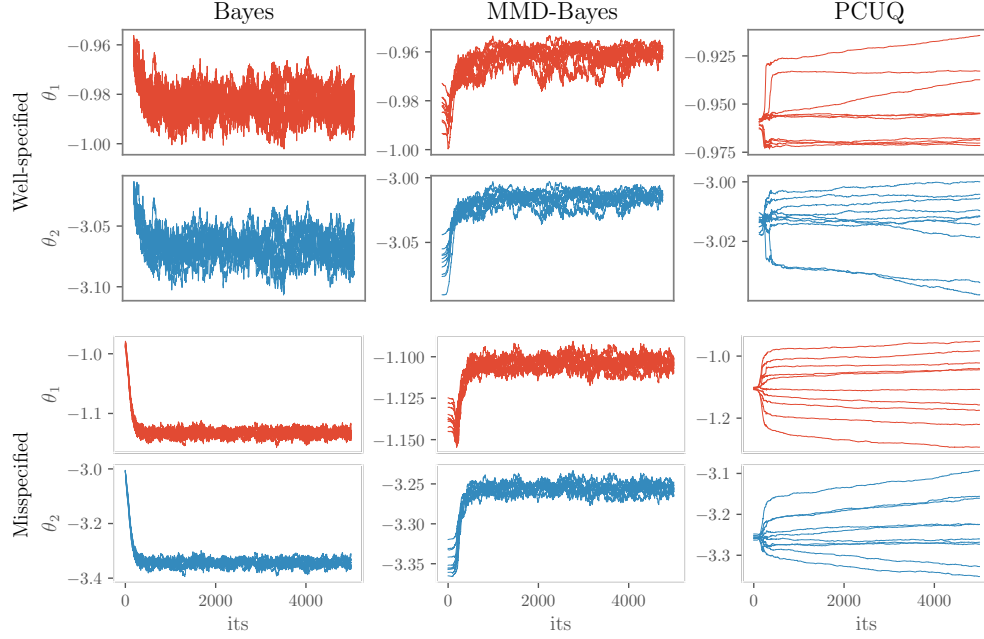


Figure 8: Lotka–Volterra model (alternative parameter settings). Convergence of sampling algorithms. Here trace plots for θ_1 (red) and θ_2 (blue) are presented for the sampling algorithms used to approximate the standard Bayesian posterior (left), the MMD-Bayes output (middle) and the proposed PCUQ method (right). The top row corresponds to the well-specified case where data were generated from the ODE model, while the bottom row corresponds to the misspecified case where data were generated from the SDE model.

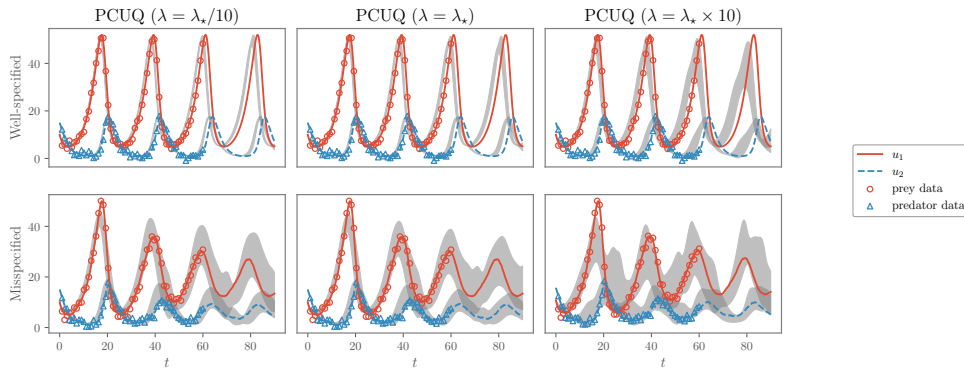


Figure 9: Lotka–Volterra Model (modified parameter settings). Investigating sensitivity to the number of particles N . The proposed gradient flow algorithm involves selecting a number of particles N , and in the main text we presented results based on $N = 10$. To assess the sensitivity to this choice, we re-computed trace plots based on the alternative choices $N = 5$ (left) and $N = 15$ (right). Here data were generated from the well-specified model.

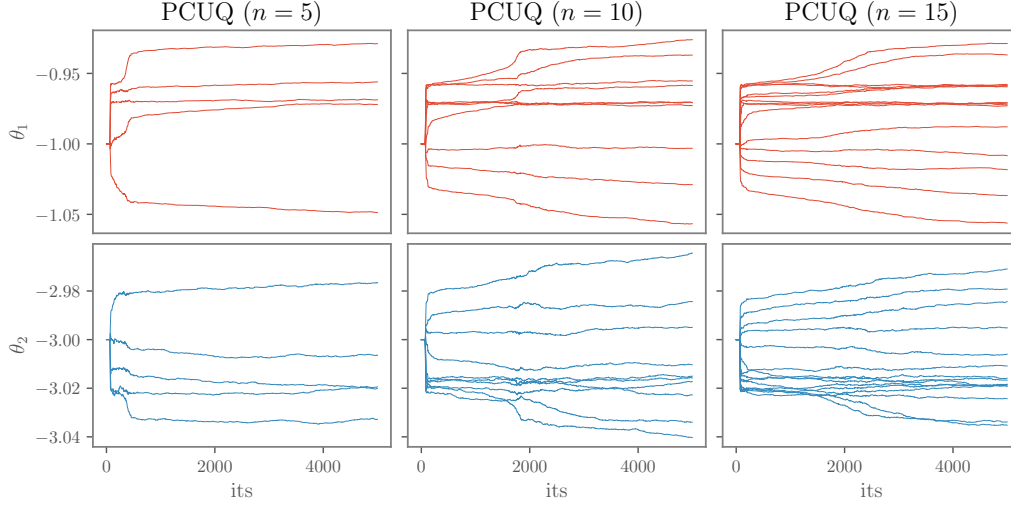


Figure 10: Lotka–Volterra Model (modified parameter settings). Investigating sensitivity to the number of particles N . The proposed gradient flow algorithm involves selecting a number of particles N , and in the main text we presented results based on $N = 10$. To assess the sensitivity to this choice, we re-computed trace plots based on the alternative choices $N = 5$ (left) and $N = 15$ (right). Here data were generated from the misspecified model.

$$\begin{aligned}
 \frac{du_1}{dx} &= f_1(u; \beta) = -\beta_1 u_1 u_2 + \beta_2 u_3 + \beta_5 u_4 \\
 \frac{du_2}{dx} &= f_2(u; \beta) = -\beta_1 u_1 u_2 + \beta_2 u_3 + \beta_{11} u_{11} \\
 \frac{du_3}{dx} &= f_3(u; \beta) = \beta_1 u_1 u_2 - \beta_2 u_3 - \beta_3 u_3 u_9 + \beta_4 u_4 \\
 \frac{du_4}{dx} &= f_4(u; \beta) = \beta_3 u_3 u_9 - \beta_4 u_4 - \beta_5 u_4 \\
 \frac{du_5}{dx} &= f_5(u; \beta) = \beta_5 u_4 - \beta_6 u_5 u_7 + \beta_7 u_8 \\
 \frac{du_6}{dx} &= f_6(u; \beta) = \beta_5 u_4 - \beta_9 u_6 u_{10} + \beta_{10} u_{11} \\
 \frac{du_7}{dx} &= f_7(u; \beta) = -\beta_6 u_5 u_7 + \beta_7 u_8 + \beta_8 u_8 \\
 \frac{du_8}{dx} &= f_8(u; \beta) = \beta_6 u_5 u_7 - \beta_7 u_8 - \beta_8 u_8 \\
 \frac{du_9}{dx} &= f_9(u; \beta) = -\beta_3 u_3 u_9 + \beta_4 u_4 + \beta_8 u_8 \\
 \frac{du_{10}}{dx} &= f_{10}(u; \beta) = -\beta_9 u_6 u_{10} + \beta_{10} u_{11} + \beta_{11} u_{11} \\
 \frac{du_{11}}{dx} &= f_{11}(u; \beta) = \beta_9 u_6 u_{10} - \beta_{10} u_{11} - \beta_{11} u_{11}
 \end{aligned}$$

Figure 11: ODE model of ERK signalling due to Kwang-Hyun et al. [2003a]. The variables u_i represent protein concentrations, as defined in Table 1, while $\beta = (\beta_1, \dots, \beta_{11})$ are non-negative rate parameters to be inferred.

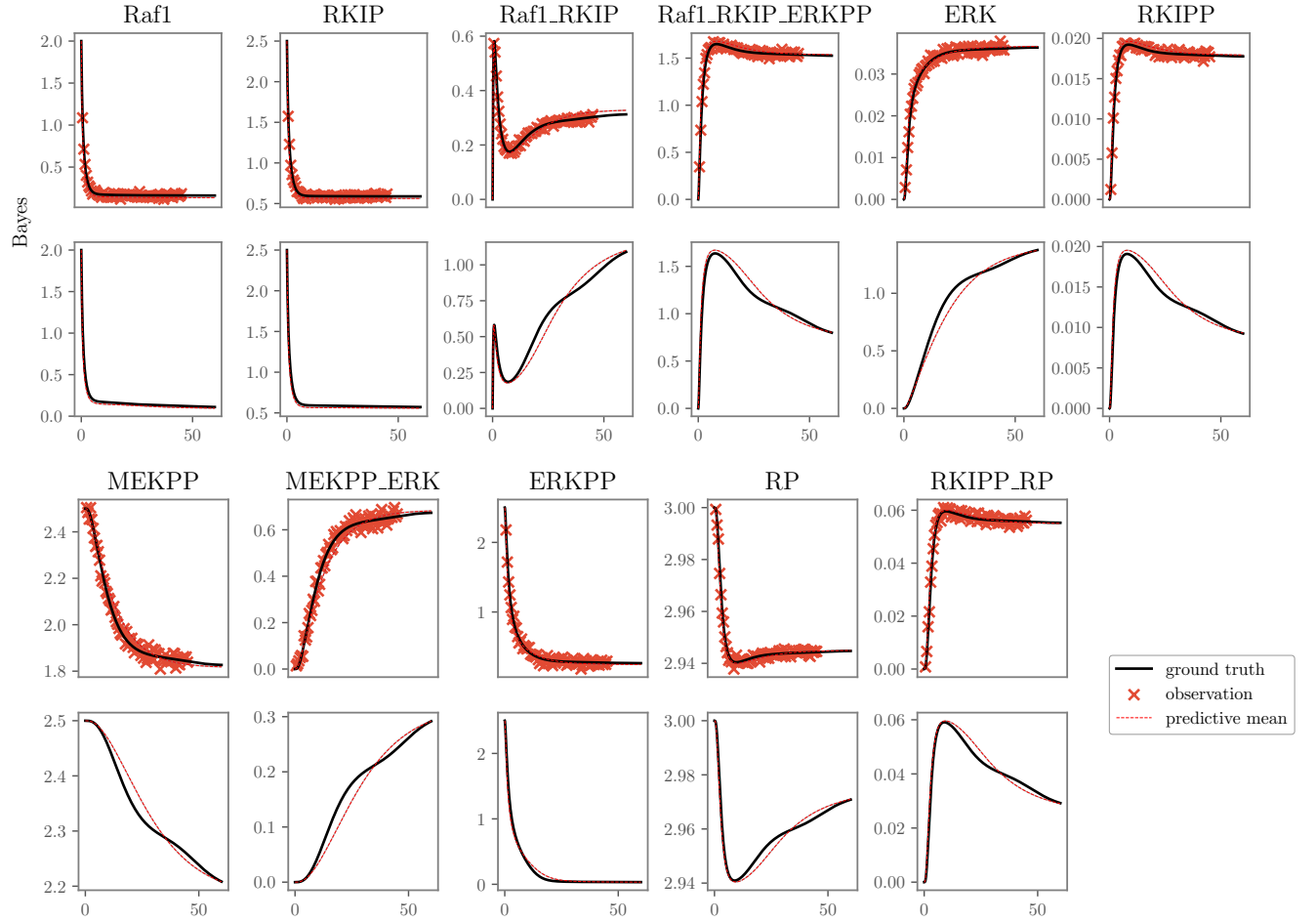


Figure 12: Full results for the ERK signalling model. Data (red crosses) were obtained as noisy observations of the system trajectory (black line) in an observational regime (top row), and the task was to predict the causal effect of a MEK inhibitor (MEKi) on ERK signalling (bottom row). Predictions produced using standard Bayesian inference were grossly over-confident. [Here the red line indicates predictive mean, while the shaded region (so small as to be difficult to see) indicates predictive quartiles.]

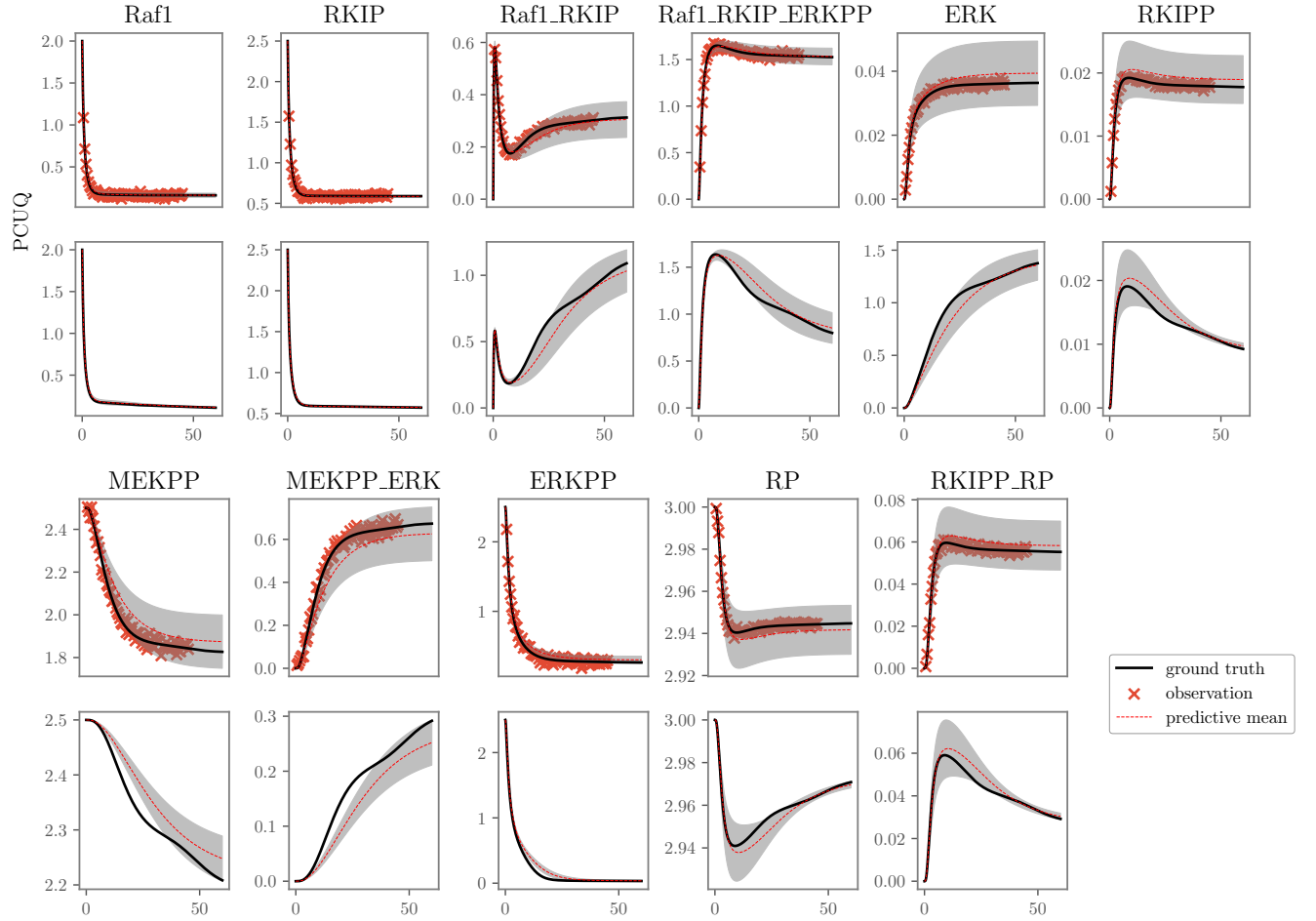


Figure 13: Full results for the ERK signalling model. Data (red crosses) were obtained as noisy observations of the system trajectory (black line) in an observational regime (top row), and the task was to predict the causal effect of a MEK inhibitor (MEKi) on ERK signalling (bottom row). Predictions produced using PCUQ enabled predictive uncertainty to be accurately quantified. [Here the red line indicates predictive mean, while the shaded region indicates predictive quartiles.]